

VICTORIA UNIVERSITY
MELBOURNE AUSTRALIA

Investigation of regeneratable biopolymer-based aerogels for heavy metal decontamination from water: Quantum chemical analysis and experimental investigation

This is the Published version of the following publication

Syeda, Hina Iqbal, Muthukumaran, Shobha and Baskaran, Kanagaratnam (2025) Investigation of regeneratable biopolymer-based aerogels for heavy metal decontamination from water: Quantum chemical analysis and experimental investigation. *Separation and Purification Technology*, 353. ISSN 1383-5866

The publisher's official version can be found at
<https://www.sciencedirect.com/science/article/pii/S1383586624020501?via%3Dihub>
Note that access to this version may require subscription.

Downloaded from VU Research Repository <https://vuir.vu.edu.au/49074/>



Investigation of regeneratable biopolymer-based aerogels for heavy metal decontamination from water: Quantum chemical analysis and experimental investigation

Hina Iqbal Syeda^{a,*}, Shobha Muthukumaran^b, Kanagaratnam Baskaran^a

^a Faculty of Science, Engineering and Built Environment, Deakin University, Victoria 3216, Australia

^b Institute for Sustainable Industries & Liveable Cities, College of Sport, Health and Engineering, Victoria University, Melbourne, VIC 3011, Australia

ARTICLE INFO

Editor: S. Deng

Keywords:

Water treatment
Adsorption
Polyglutamic acid
Sodium alginate
Cellulose nanofibers

ABSTRACT

Heavy metals pose a significant threat to human health and ecological security due to their high toxicity, mobility, and persistence in the environment. Herein, the synthesis of a novel cellulose nanofiber-based aerogel using non-toxic biopolymers such as sodium alginate and polyglutamic acid to eradicate lead, zinc, and copper from water is described. The physical characterisation and the adsorption performance of the aerogels were evaluated in both monolithic and bead configurations. The study revealed superior adsorption performance for the aerogel beads compared to the monolithic configuration. The aerogel beads achieved a maximum adsorption capacity of 171.7 mg/g, 100.0 mg/g, and 142.0 mg/g for lead, zinc, and copper respectively. The aerogel beads exhibited a higher specific surface area compared to the monolithic aerogels. The presence of functional groups including carboxyl, amino, and hydroxyl groups on the aerogels likely facilitated the adsorption through coordinate bond formation and electrostatic interactions. Density Functional Theory calculations supported the role of oxygen and nitrogen containing groups on the aerogel in capturing heavy metal ions. The aerogels displayed a remarkable regeneration ability and were reused 20 times, without any significant reduction in the adsorption performance indicating its potential as a sustainable adsorbent for heavy metals removal from water.

1. Introduction

The ever-growing need for modernisation has provoked accelerated water contamination with various pollutants such as dyes, toxic solvents, microplastics, antibiotics, pesticides, proteins, and heavy metals resulting in a disbalanced eco-system and negatively impacted human health [1]. The deposition of heavy metals in water bodies is an alarming concern due to their non-biodegradable nature which allows them to travel through the food chain and eventually accumulate in the human body. The consequences of heavy metal poisoning in the human body includes severe health conditions ranging from neurological disorders to carcinogenic effects [2]. Alternatively, the implications of heavy metals on the aquatic life are equally severe and can result in negatively impacted biodiversity [3]. The maximum permissible limits of some of the toxic heavy metals, including zinc, lead, copper, cadmium, mercury, chromium, and arsenic according to the United States Environmental Protection Agency (USEPA) are 5, 0.015, 1.3, 0.005, 0.02, 0.1, and 0.01 mg/L. In view of the detrimental health implications

of heavy metals on the human body and the eco-system, technologies such as chemical precipitation, membrane technology, electrocoagulation, ion exchange, and adsorption have been employed for the decontamination of heavy metal laden water bodies [4]. However, when considering the economic and environmental impacts, adsorption emerges as the most favourable decontamination technique due to its minimal waste generation and lower energy requirements. [5].

Due to the growing concerns over environmental protection, sustainable and bio-based adsorbents such as cellulose nanofibers have garnered significant interest in the research community. Although many adsorbents such as activated carbon, biochar, magnetic nano-adsorbents, and metal-organic framework (MOF) have been used for the elimination of heavy metals from water, some major drawbacks have been observed. For instance, activated carbon suffers from unsatisfactory regeneration and high operation expenses [6]. Biochar shows poor adsorption performance due the lack of sufficient functional groups on the surface and inadequate specific surface area [7,8]. Similarly, MOF's organic ligands are high in cost, demonstrate instability in aqueous

* Corresponding author.

E-mail address: hinaiqbs@gmail.com (H.I. Syeda).

<https://doi.org/10.1016/j.seppur.2024.128311>

Received 9 May 2024; Received in revised form 4 June 2024; Accepted 4 June 2024

Available online 6 June 2024

1383-5866/© 2024 The Authors. Published by Elsevier B.V. This is an open access article under the CC BY-NC license (<http://creativecommons.org/licenses/by-nc/4.0/>).

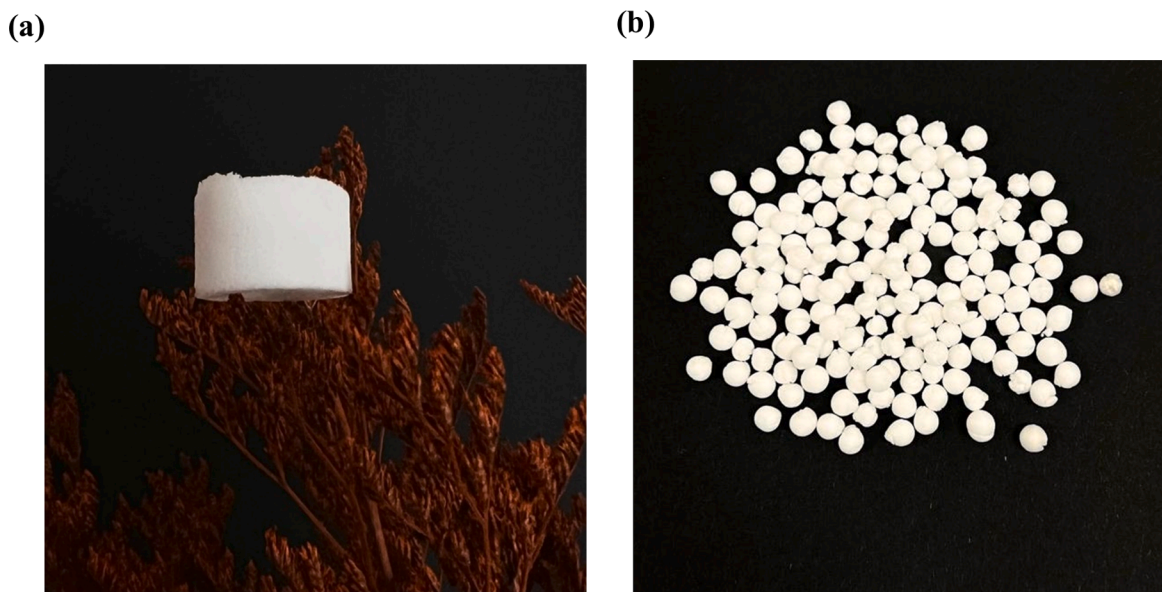


Fig. 1. (a) CNF-SP monolithic aerogel, (b) CNF-SP aerogel beads.

solutions, and present obstacles during the recovery process [9]. Most magnetic nanoparticles are not soluble in water, can suffer from aggregation and issues associated with oxidation/dissolution in an acidic medium. To address these limitations, additional solvents and toxic chemicals may be required which in turn can increase the negative environmental impact and the overall production cost [10]. Pertaining these issues, researchers have been working on improving the adsorption properties of these materials. For instance, granular activated carbon was doped with iron for the removal of lead. The adsorbent had a large surface area of $715 \text{ m}^2/\text{g}$ and an adsorption capacity of 124.3 mg/g [11]. Carbide-derived carbon has also been used for the removal of chromium from water. The adsorption capacity was notable reaching 1591.1 mg/g , under optimal conditions [12]. Recently, low cost and environmentally friendly biosorbents have also been extensively explored to remove heavy metals from water. For instance, biochar was prepared from coffee waste for the removal of cadmium and lead. The achieved adsorption capacity was 116.3 mg/g and 139.5 mg/g respectively. [13]. Rosa damascene waste was explored as another environmentally friendly adsorbent for the removal of cadmium and lead and achieved an adsorption capacity of 24.8 mg/g for lead and 24.9 mg/g for cadmium [14]. In another study, palm leaves were used to prepare biochar for the removal of lead and chromium and the adsorption capacity was 79.2 mg/g and 51.9 mg/g , respectively [15].

To alleviate concerns regarding the recyclability, challenging post-adsorption separation and environmental impact, third-generation aerogels or cellulose based aerogels are categorised as promising functional adsorbents for the decontamination of heavy metals from water. Cellulose-based aerogels possess key properties ideal for adsorbents used in water treatment, including high specific surface area, high porosity, and a stable three-dimensional structure [16]. Moreover, cellulose is the most abundantly available biopolymer with a homogenous structure that is non-toxic to the environment and can contribute towards a more sustainable approach for treating contaminated water [17]. Upon extensive investigation, it was evident that cellulose based aerogels have shown remarkable adsorption performance [5–10]. However, it was concluded that most of the studies encompassing cellulose nanofiber (CNF) based aerogels have investigated only their monolithic form. Other physical configurations, such as aerogel beads, can prove to be more effective and efficient due to their shorter diffusion path length [20]. Apart from faster kinetics, aerogel beads have a higher specific surface area that can participate in the improvement of the adsorption

capabilities of the aerogels [21]. Additionally, in a continuous flow reactor which is typically a column, aerogel beads can facilitate enhanced flow dynamics when compared to their monolithic counterpart, due to their smaller size and potential to be packed in a more uniform manner. Moreover, the regeneration performance in many studies shows a notable reduction in the removal percentage with subsequent cycles and the regeneration was not explored past a few adsorption–desorption cycles. For instance, in a study the authors used cellulose nanofiber/chitosan/montmorillonite aerogels to remove copper, lead, and cadmium from water. The aerogels were used up to five times, with the removal percentage decreasing from 100 % to 80 % in the fifth cycle [19]. In another study, sodium alginate/cellulose nanofibers/polyethyleneimine aerogels were recycled up to five times to test the removal of chromium(VI) from water. After the first cycle, the removal percentage was 82.11 %. The removal percentage after the fifth cycle was reduced to 40.11 % [51]. In another article, the recyclability of polydopamine coated nanocellulose/amyloid aerogel for lead removal was tested by conducting three adsorption–desorption cycles. The removal percentage reduced from 94.7 % in the first cycle to 82.8 % in the third cycle [22]. There is a need to further explore a suitable aerogel configuration for continuous adsorption systems with a high recyclability rate. To target sustainable water decontamination, it is essential to produce highly regeneratable materials to reduce production costs and the carbon footprint of the adsorbent. To bridge the aforementioned gaps, this study aims to prepare a highly recyclable and stable adsorbent that can be easily utilized in a continuous reactor system.

In this study, CNF-based aerogels have been employed for the decontamination of water laden with lead, zinc, and copper. With a focus on minimizing environmental impact, the CNF-based aerogels were prepared through a simple method involving the addition of non-toxic biopolymers namely, sodium alginate and polyglutamic acid to a CNF matrix. The gel was used to prepare monolithic aerogels and aerogel beads. The adsorption process was optimized by studying various experimental conditions. The research comprehensively investigated the physical characteristics, adsorption performance, and regeneration capabilities of both monolithic aerogels and aerogel beads. The mechanisms of adsorption were explored by combining experimental data and density functional theory (DFT) calculations. The novelty of this work lies in (1) the exploration of CNF aerogel beads alongside monolithic aerogels, (2) synthesizing the adsorbents by utilisation of non-toxic

biopolymers including CNF, sodium alginate, and polyglutamic acid via a simple one pot synthesis reaction, (3) 100 % shape recovery upon mechanical compression, and (4) demonstrating excellent recycling performance even after 20 cycles.

2. Materials and experimental protocols

2.1. Materials

Cellulose nanofiber (CNF) slurry with a concentration of 3 wt% was purchased from CelluloseLab. (3-glycidyoxypropyl) trimethoxysilane (GPTMS, $\geq 98\%$), zinc nitrate hexahydrate ($\text{Zn}(\text{NO}_3)_2 \cdot 6\text{H}_2\text{O}$, 98 %), copper nitrate hexahydrate $\text{Cu}(\text{NO}_3)_2 \cdot 6\text{H}_2\text{O}$ ($\geq 99\%$), lead nitrate $\text{Pb}(\text{NO}_3)_2$ ($\geq 99\%$), hydrochloric acid (HCl, 37 %), sodium hydroxide (NaOH, $\geq 98\%$), sodium acetate ($\geq 99\%$), and nitric acid (HNO_3 , 70 %), alginic acid sodium salt from brown algae, magnesium chloride (MgCl_2 , $\geq 98\%$) and sodium chloride (NaCl, $\geq 99\%$) were acquired from Sigma-Aldrich. Poly-gamma-glutamic acid (PGA, 99 %) in powder form was purchased from Xi'an Faithful BioTech Co., Ltd.

2.2. Synthesis of CNF/sodium alginate/polyglutamic acid monolithic aerogels and aerogel beads

Firstly, 1 wt% sodium alginate was prepared by mixing a certain amount of sodium alginate (SA) with ultrapure water at 70 °C for three hours. A probe-type homogenizer was used to dilute the 3 wt% CNF slurry to 1 wt% using ultrapure water. The sodium alginate solution was added to the 1 wt% CNF slurry with a weight ratio of 1:5 CNF:SA and further mixed using the ultrasonic homogenizer for 20 min to ensure the homogeneity of the mixture. 3-Glycidyoxypropyl)trimethoxysilane (GPTMS) was gradually added to the CNF/sodium alginate slurry with a 1:1 wt ratio of CNF:GPTMS and stirred for two hours. Polyglutamic acid was mixed with the CNF/SA/GPTMS solution in a 1:1 CNF:PGA weight ratio and stirred for 2 h. The final CNF slurry (CNF-SP) was placed into a mould to prepare monolithic aerogels and frozen at a temperature of $-20\text{ }^\circ\text{C}$ for 48 h. The frozen sample was freeze dried at $-86\text{ }^\circ\text{C}$ and 0.02–0.05 mbar pressure for 48 h. The aerogels cured in an oven at 60 °C for 1 hour.

To make aerogel beads, a syringe pump was used to generate droplets, which were directly plunged into liquid nitrogen for instant freezing. Once the beads were immediately frozen, they were placed in a freeze dryer at a temperature of $-86\text{ }^\circ\text{C}$ and 0.02–0.05 mbar pressure for 48 h. The aerogel beads were cured in an oven at 60 °C for 1 hour. The images of CNF-SP monolithic aerogel and CNF-SP aerogel beads are presented in Fig. 1. (a) and (b).

2.3. Characterisation of pristine CNF aerogels, CNF-SP monolithic aerogels, and CNF-SP aerogel beads

Fourier-transform infrared spectroscopy (FT-IR) was performed on the aerogels before and after adsorption using the Bruker Invenio-R in a scan range of 4000–400 cm^{-1} . Scanning electron microscopy (SEM) images were attained using Supra 55 VP (ZEISS, Germany) by coating the aerogels with a layer of platinum. The point of zero charge (pHzpc) and as well as the zeta potential measurements were obtained using the SurPASS 3 (Anton Paar). Visual MINTEQ 3.1 was used to analyse the speciation of the heavy metals in water at different pH values. The specific surface area of the aerogels was obtained using the Brunauer–Emmet–Teller (BET) method and the pore size distribution was studied using the Barrett, Joyner, and Halenda (BJH) method through the Quantachrome® ASIqwin TM. Thermogravimetric analysis (TGA) of the dried aerogels was conducted using Netzsch Libra TGA using 5 mg of samples that were heated at a rate of 10 K/min and was studied between 30–700 °C in presence of N_2 (20 ml/min). To freeze dry the samples, the Christ Beta 2–8 LSC Basic freeze dryer was used. The concentration of all the heavy metal solutions was measured using the Agilent 5900

Inductively Coupled Plasma Optical Emission spectroscopy (ICP–OES). To test the mechanical properties and structural stability of the aerogels, wet compression tests were conducted using the Instron universal testing machine.

2.4. Adsorption experiments

2.4.1. Experimental parameter optimization for CNF-SP monolithic aerogels and CNF-SP aerogel beads

The effect of pH on the adsorption efficiency of all the heavy metal solutions was investigated in a range of 2 to 6 at a heavy metal concentration of 20 mg/L. To adjust the solutions to the desired pH value, 0.1 M HCl and 0.1 M NaOH were used. The dose of the aerogels was studied in a range of 0.05 to 0.27 g for monolithic aerogels and 0.02 to 0.1 g for aerogel beads while all other factors were kept constant. The initial metal ion concentration was analysed between 20–110 mg/L under optimal conditions. All the experiments were conducted at room temperature and a shaking speed of 150 rpm. To calculate adsorption capacity (mg/g) and removal percentage (%), the following mathematical equations were used:

$$q_e = \frac{(C_0 - C_e) \times V}{m} \quad (1)$$

$$R = \frac{(C_0 - C_e)}{C_0} \times 100 \quad (2)$$

where q_e (mg/g) signifies the equilibrium adsorption capacity, R (%) denotes the removal efficiency, C_0 (mg/L) and C_e (mg/L) is the initial and equilibrium concentration, V (L) is the volume of the solutions and m (g) is the mass of aerogels.

2.4.2. Adsorption isotherm modelling

Various adsorption isotherm models, including the Langmuir, Freundlich, Temkin and Dubinin-Radushkevich models were employed to study the adsorption process. The description of the mathematical models in their linear form is represented as follows:

$$\frac{C_e}{q_e} = \frac{1}{q_{\max}} C_e + \frac{1}{K_L q_{\max}} \quad (3)$$

$$\log q_e = \log K_F + \frac{\log C_e}{n} \quad (4)$$

$$q_e = B_1 \ln A_1 + B_1 \ln C_e \quad (5)$$

$$\ln q_e = -k_{DR} \epsilon^2 + \ln q_s \quad (6)$$

$$E = \frac{1}{\sqrt{2K_{DR}}} \quad (7)$$

$$R_L = \frac{1}{1 + K_L C_0} \quad (8)$$

where q_e (mg/g) is the equilibrium adsorption capacity, q_{\max} (mg/g) represents the maximum adsorption capacity, C_e (mg/L) represents the equilibrium concentration, K_L (L/mg) is the Langmuir constant, K_F is the Freundlich constant, n is the intensity factor, $B_1 = \frac{RT}{b}$ where T (K) represents the absolute temperature (K), R ($8.314 \times 10^{-3} \text{ J mol}^{-1} \text{ K}^{-1}$) is the ideal gas constant and b is the Temkin constant (J mol^{-1}), A_T represents the Temkin binding constant (L/g), the Dubinin-Radushkevich isotherm constant in the equation is represented as k_{DR} ($\text{mol}^2 \text{ kJ}^{-2}$), q_s presents the theoretical adsorption capacity (mg/g), ϵ represents the Polanyi potential which is calculated by using $\epsilon = RT \ln(1 + 1/C_e)$, E signifies the mean adsorption free energy.

2.4.3. Adsorption kinetics modelling

The adsorption kinetics were investigated through the the pseudo-

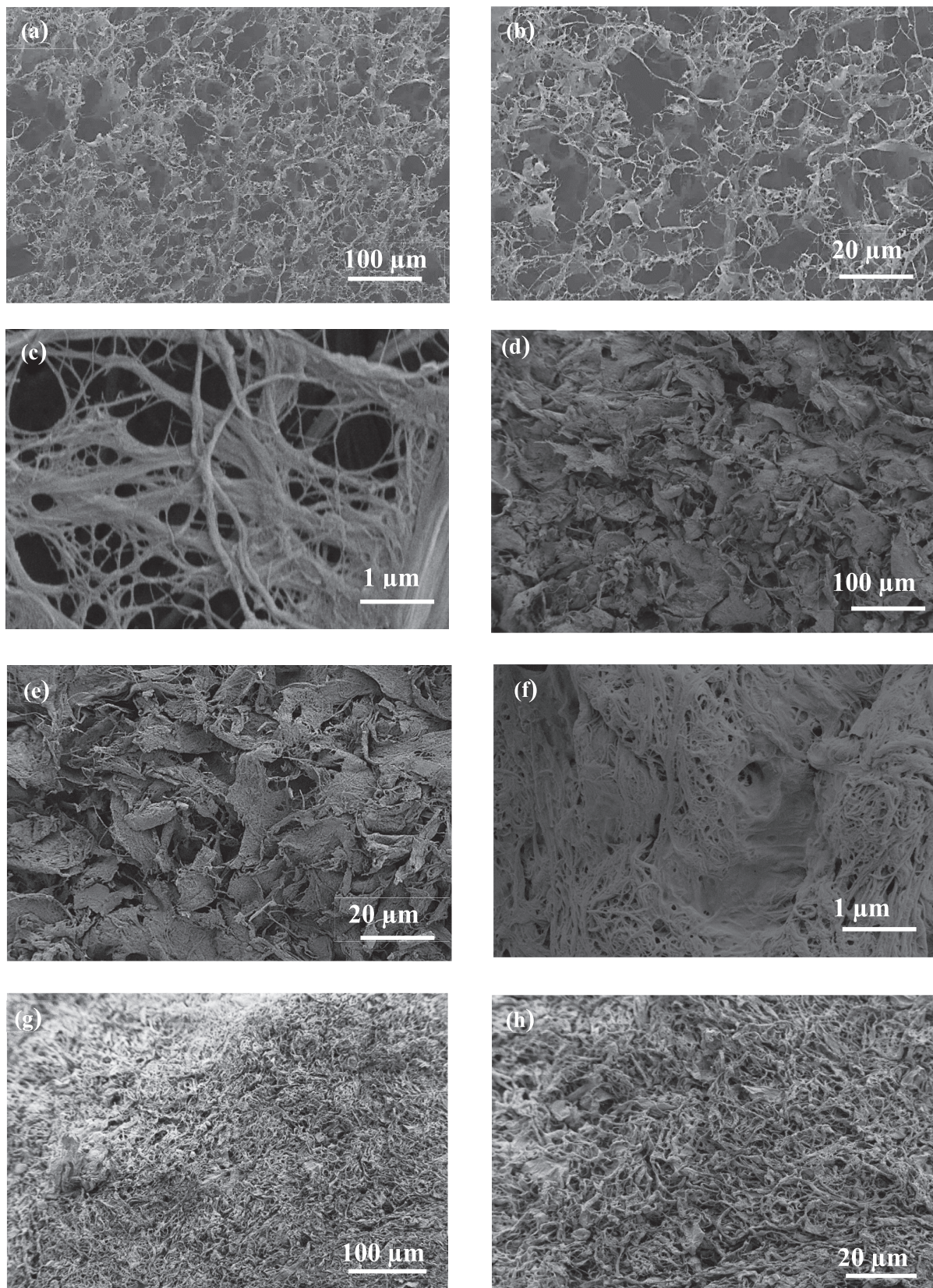


Fig. 2. SEM image of (a) pristine CNF (scale bar: 100 μm), (b) pristine CNF (scale bar: 20 μm), (c) pristine CNF (scale bar: 1 μm), (d) CNF-SP monolithic aerogels (scale bar: 100 μm), (e) CNF-SP monolithic aerogels (scale bar: 20 μm), (f) CNF-SP monolithic aerogels (scale bar: 1 μm), (g) CNF-SP aerogel beads (scale bar: 100 μm), (h) CNF-SP aerogel beads (scale bar: 20 μm), (i) CNF-SP aerogel beads (scale bar: 1 μm) (j) N_2 adsorption–desorption isotherm curve of CNF-SP monolithic aerogels (k) N_2 adsorption–desorption isotherm curve of CNF-SP aerogel beads, (l) pore size distribution of CNF-SP monolithic aerogels and aerogel beads.

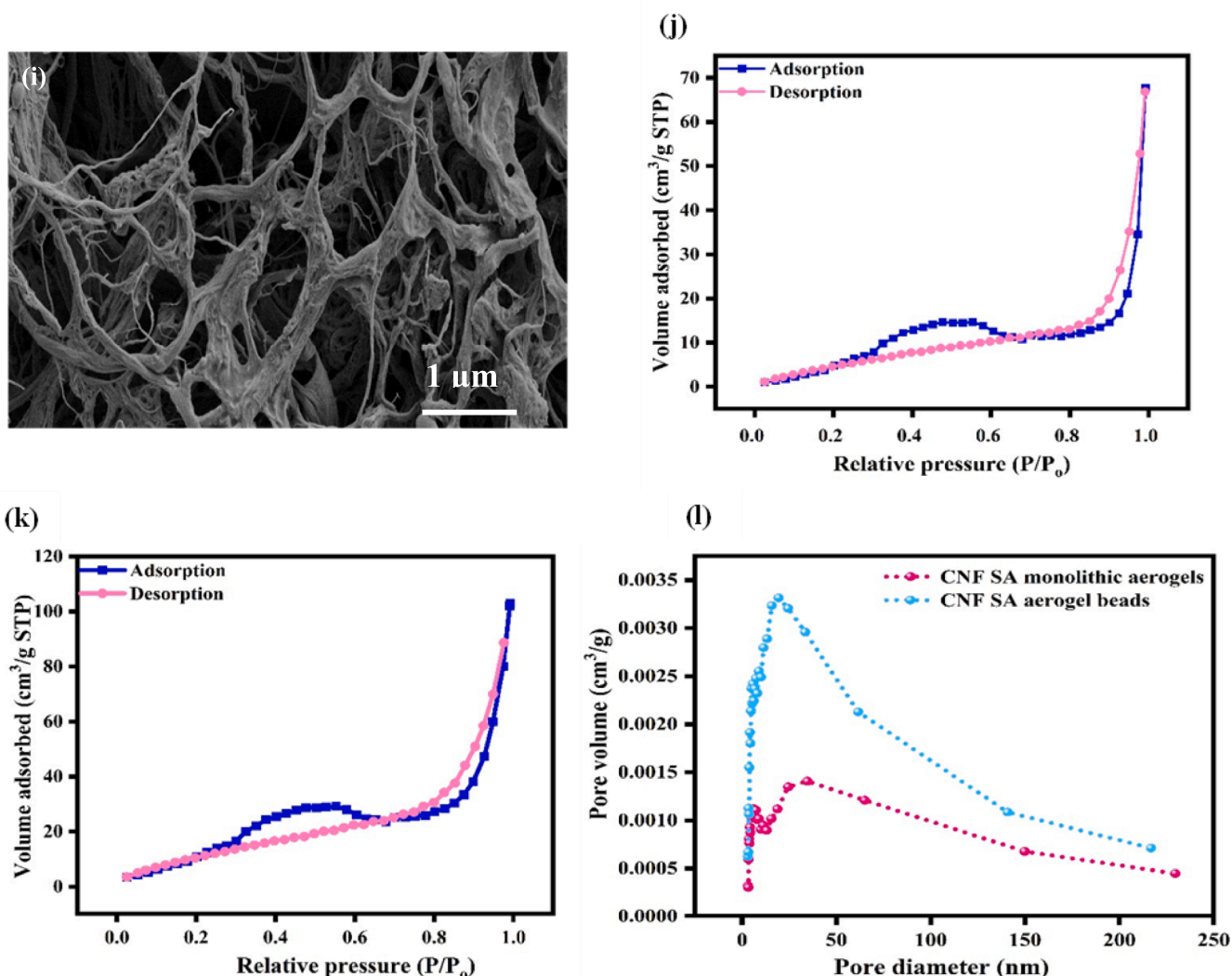


Fig. 2. (continued).

first-order (PFO) kinetic model, pseudo-second-order (PSO) kinetic model, intra- particle diffusion (IPD) model and Elovich model. These models are described in their linear form as follows:

$$\ln(q_e - q_t) = \ln q_e - k_1 t \quad (9)$$

$$\frac{t}{q_t} = \frac{1}{k_2 q_e^2} + \frac{t}{q_e} \quad (10)$$

$$q_t = k_{id} t^{1/2} + C \quad (11)$$

$$q_t = \frac{\ln \alpha \beta}{\beta} + \frac{\ln t}{\beta} \quad (12)$$

where the PFO rate constant is described as k_1 (1/min), the contact time is represented as t (min), q_t is the adsorption capacity at the respective time, k_2 ($\text{gmg}^{-1}\text{min}^{-1}$) represents the PSO rate constant, k_{id} ($\text{mg/g}^1 \text{min}^{1/2}$) represents the intraparticle diffusion rate constant, C is constant and is associated with the thickness of the boundary layer, α is the initial adsorption rate (mg/g min), and β (g/mg) is the Elovich adsorption constant.

2.4.4. Effect of co-existing ions

The influence of 0.001–0.1 M NaCl and MgCl₂ on the adsorption of 20 mg/L of all the heavy metal ions using CNF-SP monolithic aerogels

and CNF-SP aerogel beads was studied at optimal conditions achieved from the optimization studies. A sample reading was extracted for analysis after the system reached equilibrium and was analysed using the ICP-OES.

2.4.5. Multi-metal adsorption studies and aerogel efficiency comparison analysis

To investigate the adsorption performance of the CNF-SP monolithic aerogels and CNF-SP aerogel bead in a multi-metal simulated system a certain concentration of nitrates, phosphates, calcium, magnesium, ammonia were combined with 20 mg/L of the heavy metal ions. All the tests were conducted at optimal conditions. The performance of the aerogels was also compared to commercial activated carbon that was used to remove heavy metals under the same operating conditions as well as other adsorbents and technologies in literature.

2.5. Reusability assessment

To explore the reusability of the CNF-SP monolithic aerogels and CNF-SP aerogel beads, 1 M citric acid was used as a desorbing agent. The spent aerogels were mixed with the citric acid solution in an orbital shaker at 150 rpm for 2 h. Next, the aerogels were thoroughly rinsed several times with ultrapure water for neutralisation. The pH was adjusted using sodium acetate. The aerogels were subjected to 20

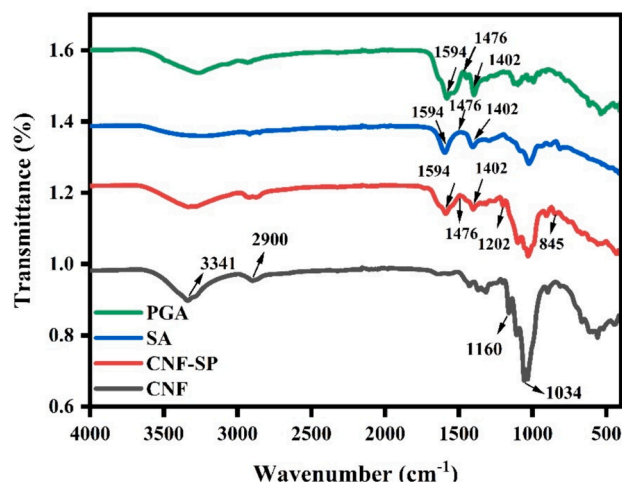


Fig. 3. FTIR spectra of pristine CNF aerogels, CNF-SP monolithic aerogels, PGA, and SA.

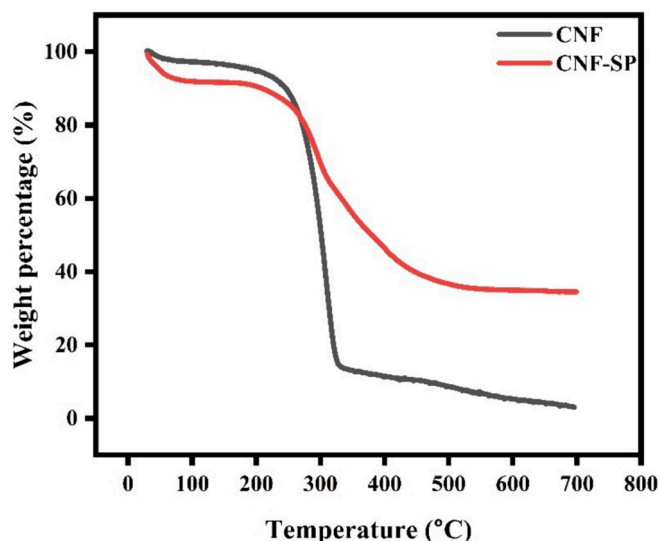


Fig. 4. TGA analysis of pristine CNF aerogels and CNF-SP monolithic aerogels.

continuous adsorption–desorption cycles.

$$\text{Desorption \%} = \frac{\text{Amount desorbed in the solution } \left(\frac{\text{mg}}{\text{g}}\right)}{\text{Amount adsorbed by the adsorbent } \left(\frac{\text{mg}}{\text{g}}\right)} \times 100 \quad (13)$$

2.6. Density functional theory calculations

The adsorption process was further studied using the ORCA 5.0.3 software through the density functional theory (DFT) calculations. To calculate the single point energies, the B3LYP and LANL2DZ basis set was used after geometry optimization. The interaction energies were calculated by using the following equation.

$$E_{\text{ads}} = E_{\text{M@CNF-SP}} - (E_{\text{M}} + E_{\text{CNF-SP}}) \quad (14)$$

where $E_{\text{M@CNF}}$, E_{CNF} , and E_{M} are the energies of complexes, CNF-SP aerogel, and metal ions respectively.

Various properties of the complexes such as E_{gap} , chemical hardness and chemical softness were calculated using the following equations respectively:

$$E_{\text{gap}} = E_{\text{L}} - E_{\text{H}} \quad (15)$$

$$\eta = \frac{E_{\text{L}} - E_{\text{H}}}{2} \quad (16)$$

$$S = \frac{1}{\eta} \quad (17)$$

where, E_{H} represents the energy exhibited by the highest occupied molecular orbital. Alternatively, E_{L} represents the energy of lowest unoccupied molecular orbital.

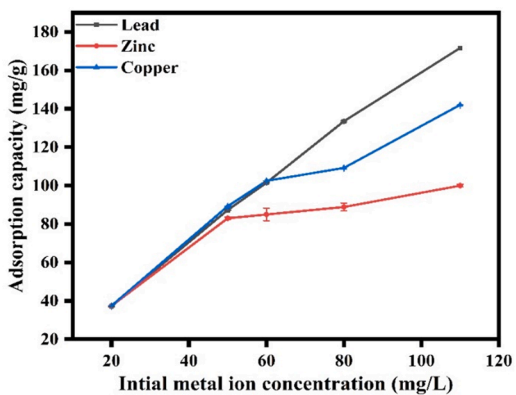
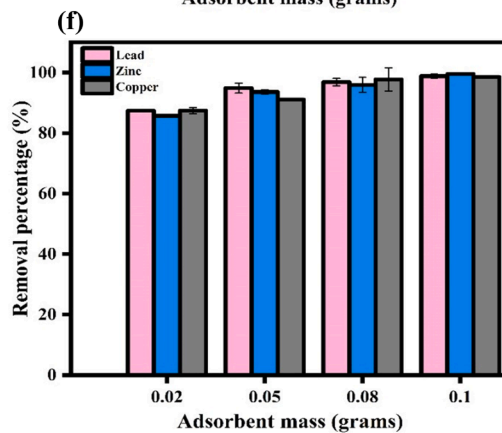
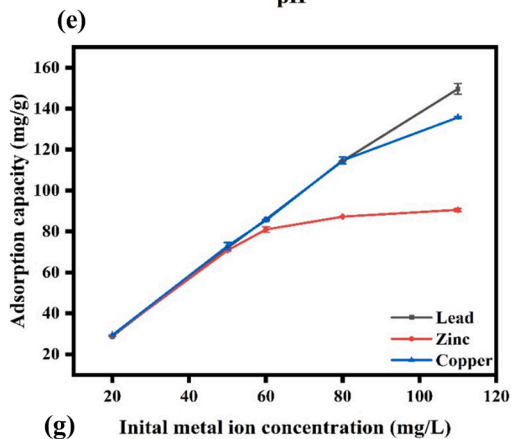
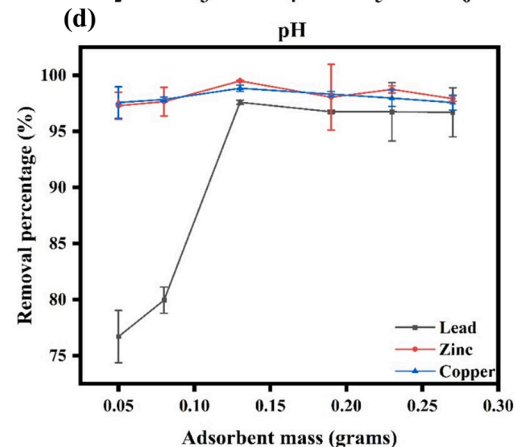
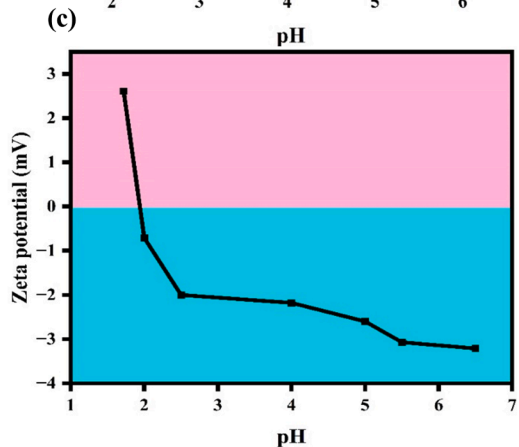
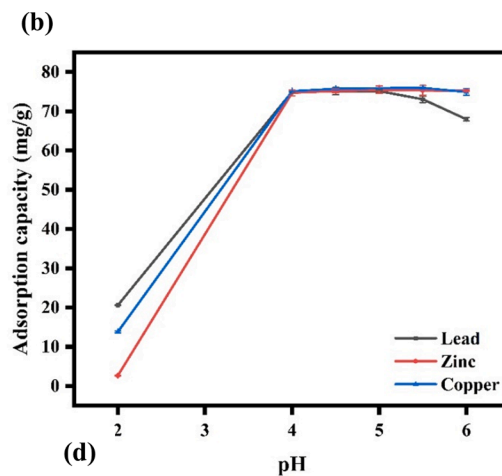
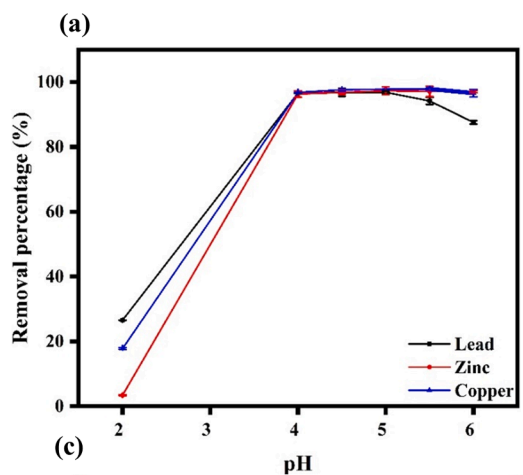
3. Results and discussion

3.1. Structural and chemical characterisation of pristine CNF aerogels, CNF-SP monolithic aerogels, and CNF-SP aerogel beads

To explore the morphological aspect of the pristine CNF aerogels, CNF-SP monolithic aerogels and CNF-SP aerogel beads, SEM images were captured. As presented in Fig. 2. (a), (b), and (c), the pristine CNF aerogels demonstrated a loosely interconnected structure with a heterogeneous distribution of pores. The CNF-SP monolithic aerogels depict a tightly bounded and interconnected flaky sheet-like structure with abundant pores as presented in Fig. 2. (d), (e), and (f). CNF-SP monolithic aerogels were prepared by freezing the CNF-SP gel in a freezer at -20 °C. This type of freezing technique facilitates the formation of random and irregular ice crystals. Therefore, the development of the porous structure of the aerogels upon sublimation is irregular [23].

Alternatively, in the case of CNF-SP aerogel beads, the gel was dropped directly into liquid nitrogen, causing rapid formation of ice crystals. Clearly, Fig. 2. (g), (h), and (i) proves that the CNF-SP aerogel beads depicted a highly porous, interconnected structure with a comparatively even distribution of pores. From the pictorial comparison of the SEM images of pristine CNF aerogels, CNF-SP monolithic aerogels, and CNF-SP aerogel beads, it is evident that crosslinking with PGA and SA, as well as the freezing techniques had a notable effect on the structure of the aerogels. The crosslinking reaction facilitated the formation of weakly connected fibrils in the case of the pristine CNF aerogels. For CNF-SP monolithic aerogels, the crosslinking between the functional groups led to the formation of uniform and densely connected flake like sheets, as a result of differential contraction and expansion of the ice crystals whereas, the crosslinking in the CNF-SP aerogel beads created strongly connected fibres as a result of rapid solidification and minimal redistribution during freezing. To further confirm these results, BET surface area analysis was conducted on CNF-SP monolithic aerogels and CNF-SP aerogel beads. According to the results, the specific surface area of CNF-SP monolithic aerogels was calculated to be $227 \text{ m}^2/\text{g}$ whereas the specific surface area of CNF aerogel beads was found to be $258 \text{ m}^2/\text{g}$ as seen in Fig. 2. (j) & (k). The larger specific surface area of the CNF-SP aerogel beads can be visualised through the SEM images. Interestingly, as shown in Fig. 2 (l), both the monolithic aerogel and aerogel beads exhibited pores mostly in the mesopore region with a pore diameter in the range of 2–50 nm alongside fewer pores present in the micropore and macropore region, with diameters varying between less than 2 nm and greater than 50 nm respectively. The monoliths depicted the presence of more uniform mesopores compared to the aerogel beads. This could be due to the difference in the freezing technique. The slow and controlled freezing in the case of monoliths resulted in the formation of more consistent mesopores when compared to the aerogel beads for which the freezing was rapid and resulted in the formation of a wider range of mesopores and macropores.

The spectra acquired from the FTIR analysis of the pristine CNF aerogels, CNF-SP monolithic aerogel, SA, and PGA are presented in Fig. 3. The FTIR spectra of the pristine CNF aerogels depicted typical peaks associated with cellulose at 3341 cm^{-1} , 2900 cm^{-1} , 1160 cm^{-1} , 1034 cm^{-1} and represents the O–H stretching vibration, C–H stretching vibration, –C–O stretching and the C–O–C stretching of the pyranose ring in the CNFs [24]. Peaks noted at 1202 cm^{-1} and 845



(caption on next page)

Fig. 5. Influence of experimental factors (a) Influence of pH on the removal percentage of lead, zinc, and copper (Co = 20 mg/L, Dose = 0.05 g, T = 25 °C) (b) Influence of pH on the adsorption capacity of lead, zinc, and copper (Co = 20 mg/L, Dose = 0.05 g, T = 25 °C) (c) Representation of zeta potential measurements of CNF-SP aerogels, (d) Influence of aerogel mass on the percentage removal of lead, zinc, and copper using CNF-SP monolithic aerogels (Lead: Co = 20 mg/L, pH = 5, T = 25 °C; Zinc: Co = 20 mg/L, pH = 5.5, T = 25 °C; Copper: Co = 20 mg/L, pH = 5.5, T = 25 °C), (e) Influence of initial metal ion concentration of lead, zinc, and copper using CNF-SP monolithic aerogels (Lead: Co = 20 mg/L, pH = 5, Dose = 0.13 g, T = 25 °C; Zinc: Co = 20 mg/L, pH = 5.5, Dose = 0.13 g, T = 25 °C; Copper: Co = 20 mg/L, pH = 5.5, Dose = 0.13 g, T = 25 °C) (f) Influence of aerogel mass on the removal percentage of lead, zinc, and copper using CNF-SP aerogel beads (Lead: Co = 20 mg/L, pH = 5, T = 25 °C; Zinc: Co = 20 mg/L, pH = 5.5, T = 25 °C; Copper: Co = 20 mg/L, pH = 5.5, T = 25 °C), (g) Influence of initial metal ion concentration of lead, zinc, and copper using CNF-SP aerogel beads (Lead: Co = 20 mg/L, pH = 5, Dose = 0.1 g, T = 25 °C; Zinc: Co = 20 mg/L, pH = 5.5, Dose = 0.1 g, T = 25 °C; Copper: Co = 20 mg/L, Dose = 0.1 g, pH = 5.5, T = 25 °C).

cm^{-1} can be associated with the epoxy groups from GPTMS confirming its role in the crosslinking reaction [25]. Overlapping peaks originating from SA and PGA can be observed in the CNF-SP monolithic aerogel spectrum at 1594 cm^{-1} and 1402 cm^{-1} indicating the successful introduction of SA and PGA into the structure of CNFs. In the spectrum of the pristine SA, these peaks correspond to the COO^- group. The peak at 1594 cm^{-1} can be recognized as the $\text{C}=\text{O}$ stretching vibration of the amide II band in PGA. The peak at 1402 cm^{-1} in PGA was also associated with the amide II band in pristine PGA. The peak at 1476 cm^{-1} in the spectrum of PGA can be credited to the $\text{N}-\text{H}$ bending and the $\text{C}-\text{N}$ stretching vibrations of the $-\text{CO}-\text{NH}-$ group [26].

TGA analysis uncovered differences in thermal stability between the pristine CNF aerogels and the CNF-SP monolithic aerogels. In the case of both the aerogels, as shown in Fig. 4, a multi-step decomposition process can be observed. The weight loss in the initial stages, below $180 \text{ }^\circ\text{C}$, can be attributed to the evaporation of absorbed water. Notably, this initial mass loss is higher for the CNF-SP monolithic aerogels when compared to the pristine aerogels suggesting that the CNF-SP monolithic aerogels have the ability to preserve more moisture. The drastic weight loss between $225 \text{ }^\circ\text{C}$ and $328 \text{ }^\circ\text{C}$ for pristine CNF aerogels can be ascribed to the decomposition of the cellulosic structure, including the breakdown of cellulose through depolymerisation of cellulose along with the release and decomposition of volatile products. The second stage for the CNF-SP monolithic aerogels is from $180 \text{ }^\circ\text{C}$ to $480 \text{ }^\circ\text{C}$, indicating further decomposition of the volatile substances. Interestingly, the weight loss in the first stage occurs quicker for the CNF-SP monolithic aerogels when compared to the pristine CNF aerogels, whereas, the overall mass loss is higher for the pristine CNF-aerogels. The quicker degradation of the CNF-SP monolithic aerogels in the initial stage could be because of the introduction of more chemically reactive functional groups such as amino and carboxyl groups in the matrix.

To further test the mechanical strength of the CNF-SP monolithic aerogels and aerogel beads, 10 wet compression cycles were conducted. At a compressive strain of 50 % and 80 %, the maximum compressive stress for the CNF-SP monolithic aerogels was found to be 10 kPa and 150 kPa, respectively. The maximum compressive stress of the CNF-SP aerogel beads at 50 % and 80 % compressive strain was found to be 10 kPa and 40 kPa, respectively. Evidently, the aerogel beads had a lower compressive stress at 80 %. This is because the aerogel beads are much smaller in size and may exhibit a lower load-bearing capacity at higher strains. As previously mentioned, the specific surface area of the aerogel beads was higher than the monolithic aerogels. The higher specific surface area could lead to internal friction and shearing effects which could also contribute to the lower compressive stress. The height and diameter of the aerogels were measured before and after the 10 compression cycles, and it was found that the aerogels could make a 100

% shape recovery presenting its remarkable ability to regain its shape. When compared to the pristine CNF aerogels, which collapsed when in contact with water, CNF-SP monolithic aerogels and aerogel beads evidently showed extraordinary strength and structural integrity after the crosslinking process through their 100 % shape recovery even after several compression cycles. The introduction of biopolymers and initiating a crosslinking reaction with GPTMS blocks the production of further hydrogen bonding and therefore allows the interconnected network to spring back to its original structure [18,27].

4. Effect of experimental factors on CNF-SP monolithic aerogels and CNF-SP aerogel beads

4.1. The impact of pH on the removal percentage of lead, zinc, and copper from water

The pH optimization is essential as it dictates the form in which the functional groups will be present for adsorption and influences the chemistry of the heavy metal ions in water. In this study, the effect of pH on the removal percentage and adsorption capacity of all the heavy metals was studied in a range of 2 to 6, as denoted in Fig. 5. (a) and (b). Clearly, the adsorption performance was unsatisfactory at low pH values. At lower pH values, lead, zinc, and copper mostly exist as Pb^{2+} , Zn^{2+} and Cu^{2+} as shown in Fig. S1. The dominance of H^+ ions at lower pH facilitates competition between H^+ and Pb^{2+} , Zn^{2+} , and Cu^{2+} ions [28]. Moreover, due to the presence of the functional groups such as the carboxyl, hydroxyl, and amine groups originating from the structure of the CNFs, SA, and PGA in their protonated state, the adsorption process is impacted negatively. The protonation of the functional groups equips them with a positive charge and facilitates electrostatic repulsion with the heavy metal ions, thereby preventing efficient adsorption from occurring. Alternatively, at higher pH values, deprotonation of the functional groups will take place, and they will gain a negative charge. The deprotonated functional groups can electrostatically interact with the heavy metal ions. Moreover, the competitive adsorption between H^+ , ions and heavy metal ions for the active sites will reduce and thereby increase the removal percentage of the heavy metal ions [29]. Additionally, at higher pH values, the presence of excessive insoluble hydroxide species can mitigate the adsorption effect significantly [30]. The zeta potential of the adsorbent is an essential factor that can describe the surface charge and its influence on the adsorption process. According to Fig. 5. (c), the point of zero charge of the adsorbent was ~ 1.93 . This means that the surface charge is positive at pH values less than 1.93 and negative at pH values greater than 1.93. The negative surface charge favours the adsorption of cations and therefore, an increase in adsorption is observed as the pH increases [31]. The maximum adsorption

Table 1

Adsorption kinetic data obtained by fitting the experimental data into different adsorption kinetic models for CNF-SP monolithic aerogels.

Metal ions	Pseudo-first-order constants			Pseudo-second-order constants			Intra-particle diffusion constants			Elovich model			Experimental q_e (mg/g)
	Calculated q_e (mg/g)	K_1	R^2	Calculated q_e (mg/g)	K_2	R^2	K_{id}	C	R^2	α	β	R^2	
Lead	31.2	4.8×10^{-5}	0.96	31.6	0.028	0.99	9.9	1.1	0.95	3.0	0.2	0.99	28.9
Zinc	3.3	2.7×10^{-5}	0.23	30.3	0.078	0.99	27.1	0.1	0.12	18.0	0.2	0.83	29.0
Copper	5.7	2.7×10^{-5}	0.34	31.3	0.051	0.99	13.9	1.0	0.72	0.9	0.2	0.86	29.1

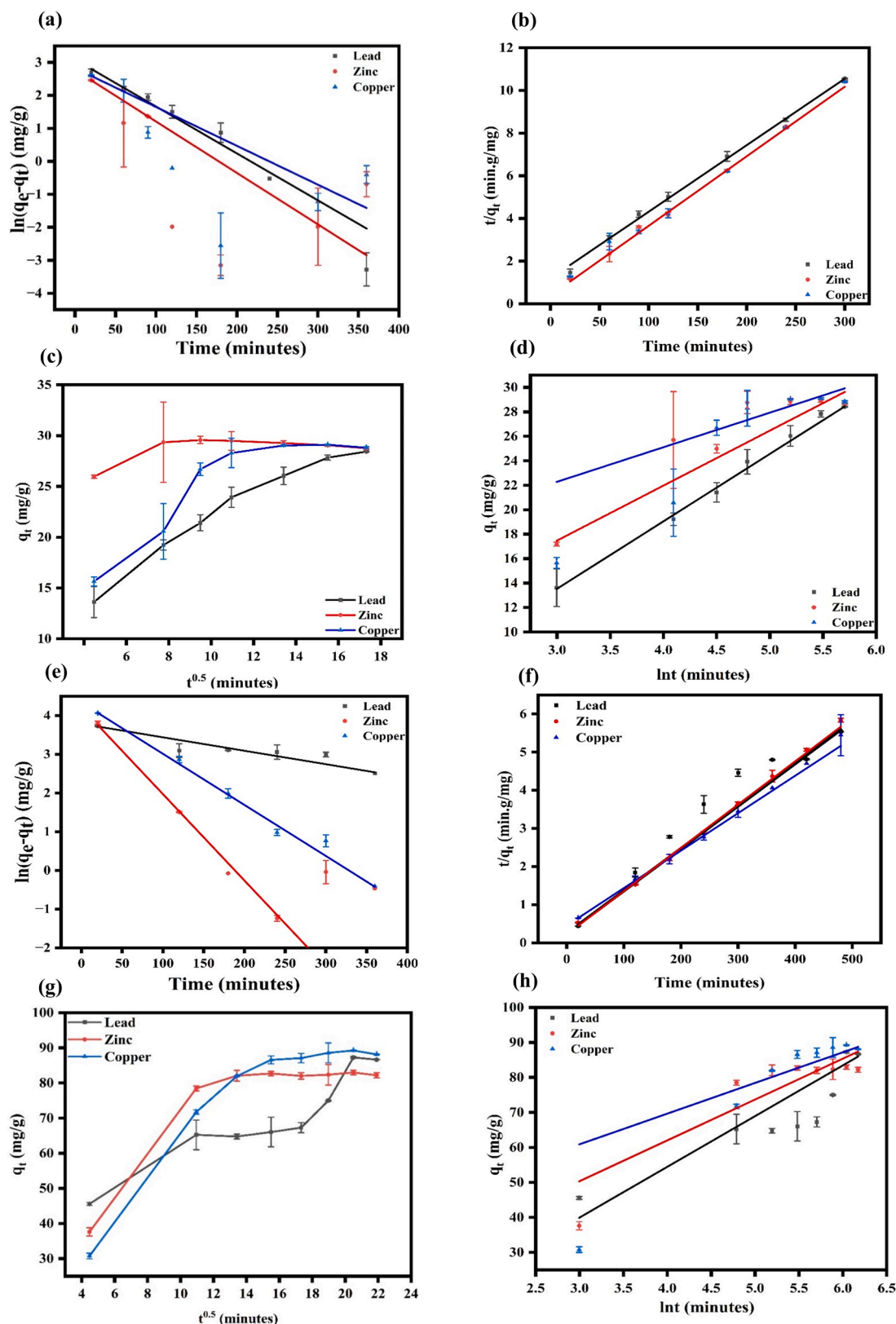


Fig. 6. (a) PFO kinetic model fitting for lead, zinc, and copper using CNF-SP monolithic aerogels, (b) PSO kinetic model fitting for lead, zinc, and copper using CNF-SP monolithic aerogels, (c) IPD kinetic model fitting for lead, zinc, and copper using CNF-SP monolithic aerogels (d) Elovich kinetic model fitting for lead, zinc, and copper using CNF-SP monolithic aerogels at (Lead: Co = 20 mg/L, pH = 5, Dose = 0.13 g, T = 25 °C; Zinc: Co = 20 mg/L, pH = 5.5, Dose = 0.13 g T = 25 °C; Copper: Co = 20 mg/L, pH = 5.5, Dose = 0.13 g, T = 25 °C), (e) PFO kinetic model fitting for lead, zinc, and copper using CNF-SP aerogel beads, (f) PSO kinetic model fitting for lead, zinc, and copper using CNF-SP aerogel beads, (g) IPD kinetic model fitting for lead, zinc, and copper using CNF-SP aerogel beads, (h) Elovich kinetic model fitting for lead, zinc, and copper using CNF-SP aerogel beads at (Lead: Co = 20 mg/L, pH = 5, Dose = 0.1 g, T = 25 °C; Zinc: Co = 20 mg/L, pH = 5.5, Dose = 0.1 g, T = 25 °C; Copper: Co = 20 mg/L, pH = 5.5, Dose = 0.1 g, T = 25 °C).

Table 2

Adsorption kinetic data obtained by fitting the experimental data into different adsorption kinetic models for CNF-SP aerogel beads.

Metal ions	Pseudo-first-order constants			Pseudo-second-order constants			Intra-particle diffusion constants			Elovich model			Experimental q_e (mg/g)
	Calculated q_e (mg/g)	K_1	R^2	Calculated q_e (mg/g)	K_2	R^2	K_{id}	C	R^2	α	β	R^2	
Lead	39.2	8×10^{-6}	0.79	91.7	0.017	0.94	35.5	2.2	0.87	22.1	0.085	87.3	
Zinc	22.3	3.3×10^{-5}	0.63	85.9	0.068	0.99	42.1	2.2	0.60	16.2	0.071	83.0	
Copper	75.9	3.6×10^{-5}	0.98	96.9	0.027	0.99	29.7	3.1	0.77	6.0	0.053	89.2	

Table 3

Adsorption isotherm parameters for the adsorption of lead, zinc, and copper on CNF-SP monolithic aerogels.

Isotherm model	Lead	Zinc	Copper
Langmuir	q_m (mg/g) = 163.93 R_L = 0.0071–0.038 R^2 = 0.99	q_m (mg/g) = 91.32 R_L = 0.0055–0.029 R^2 = 0.99	q_m (mg/g) = 142.25 R_L = 0.0074–0.039 R^2 = 0.99
Freundlich	K_F = 78.93 $1/n$ = 0.38 R^2 = 0.96	K_F = 49.75 $1/n$ = 0.19 R^2 = 0.75	K_F = 66.49 $1/n$ = 0.33 R^2 = 0.84
Temkin	B_T (J/mol) = 27.19 A_T (L/g) = 27.51 R^2 = 0.94	B_T (J/mol) = 10.73 A_T (L/g) = 176.04 R^2 = 0.85	B_T (J/mol) = 23.11 A_T (L/g) = 27.53 R^2 = 0.91
Dubinin–Radushkevich	q_s (mg/g) = 108.85 K_{Dr} (mol ² /kJ ²) = 3.42×10^{-8} E = 3823.85 R^2 = 0.82	q_s (mg/g) = 83.73 K_{Dr} (mol ² /kJ ²) = 5.24×10^{-7} E = 976.30 R^2 = 0.97	q_s (mg/g) = 105.75 K_{Dr} (mol ² /kJ ²) = 4.99×10^{-8} E = 3163.76 R^2 = 0.85

occurred at a pH value of 5, 5.5, and 5.5 for lead, zinc, and copper, respectively.

4.2. The effect of aerogel dose and initial metal ion concentration on the removal efficiency of lead, zinc, and copper from water

To determine the maximum adsorption efficiency of the aerogels, the dose of CNF-SP monolithic aerogels was varied from 0.05 to 0.27 g as shown in Fig. 5. (d). According to the results, when the dose of the aerogels was increased between 0.05 g and 0.13 g for all the heavy metals, the removal percentage increased. The increase in the adsorbent dose from 0.05 to 0.13 g provided a larger number of active sites and surface area for adsorption, inherently increasing the adsorbate-adsorbent interaction [32]. Any further increase in the dose did not significantly increase the removal efficiency. This trend can be attributed to the saturation of all the adsorption sites present on the aerogels [33]. For the aerogel beads, the dose was varied from 0.02 to 0.1 g. A trend similar to the monolithic aerogels was observed when the aerogel beads were used where an increase in the removal percentage was observed when the dose of the aerogels was increased with the maximum removal percentage at 0.1 g for lead, zinc, and copper being 98.85 %, 99.55 %, and 98.57 %, respectively as shown in Fig. 5. (f).

The effect of initial metal ion concentration on the adsorption capacity was investigated in a concentration range of 20 to 110 mg/L. The results depicted that the adsorption capacity of all the heavy metal ions increased as the initial metal ion concentration increased for the CNF-SP monolithic aerogels as show in Fig. 5. (e). This is because with an increase in the initial metal ion concentration, the concentration gradient between the solution and the surface of the adsorbent increases and the driving force is higher [34]. The maximum adsorption capacity was 149.6 mg/g, 90.5 mg/g, and 135.7 mg/g for lead, zinc, and copper,

respectively, in the range of 20 to 110 mg/L. When using the aerogel beads, it was observed that the adsorption capacity also increased when the initial heavy metal ion concentration in solution was increased as presented in Fig. 5. (g). The maximum adsorption capacity for the aerogel beads was 171.7 mg/g, 100.0 mg/g, and 142.0 mg/g for lead, zinc, and copper respectively.

5. Adsorption kinetics for CNF-SP monolithic aerogels and CNF-SP aerogel beads

The adsorption kinetics and adsorption mechanisms of the adsorption process were analysed by fitting the experimental data into the pseudo-first-order kinetics, pseudo-second-order kinetics, intraparticle diffusion, and Elovich model for the CNF-SP monolithic aerogels and aerogel beads. According to the R^2 results of the monolithic aerogels presented in Table 1, and Fig. 6. (a), (b), (c), and (d) the linearity of the plots for pseudo-first-order, Elovich, and intraparticle diffusion model were lower than that of the pseudo-second-order model, for zinc and copper. For the monolithic aerogels, the adsorption of zinc and copper ions followed the pseudo-second-order kinetic model whereas lead followed the Elovich and the pseudo-second-order kinetic model. The pseudo-second-order kinetic and Elovich model indicates that adsorbate-adsorbent interaction took place through chemisorption [35]. Additionally, the Elovich model suggests that chemisorption was the ruling adsorption mechanism in the process. Moreover, this conclusion refers to the heterogeneous diffusion process that is directed by the reaction rate and diffusion factor [36]. According to Table 2 and the plots of the aerogel beads in Fig. 6. (e), (f), (g) and (h), the pseudo-second-order was best fitted for all the heavy metals. Moreover, the plot of the intra-particle diffusion for the aerogel beads and monolithic aerogels does not pass through the origin, indicating that diffusion is not the sole rate-limiting step and other steps such as film diffusion and pore diffusion may be involved in the adsorption process.

6. Adsorption isotherms for CNF-SP monolithic aerogels and CNF-SP aerogel beads

To attain a better grasp of the interaction dynamics between the aerogels and the heavy metal solution, as well as the adsorption mechanisms, various adsorption isotherm models were explored. The experimental data obtained for CNF-SP monolithic aerogels and aerogel beads was modelled using the Langmuir, Freundlich, Temkin, and Dubinin-Radushkevich isotherm models. From the results presented in Table 3 and the graphical plots in Fig. 7. (a), (b), (c), and (d), it is evident that in the case of CNF-SP monolithic aerogels, the most prominent R^2 value was obtained from the Langmuir isotherm model and therefore it could adequately describe the experimental data in this work. The Langmuir isotherm model reflects that the adsorption occurs on a homogeneous surface and occurs in a single molecular layer or monolayer. Moreover, the R_L values were in the range of 0.0055–0.039, indicating that the adsorption process was favourable. Alternatively, as presented in Table 4 and Fig. 7. (e), (f), (g), and (h), the experimental data of CNF-SP aerogel beads for lead agreed with the assumptions of the Freundlich

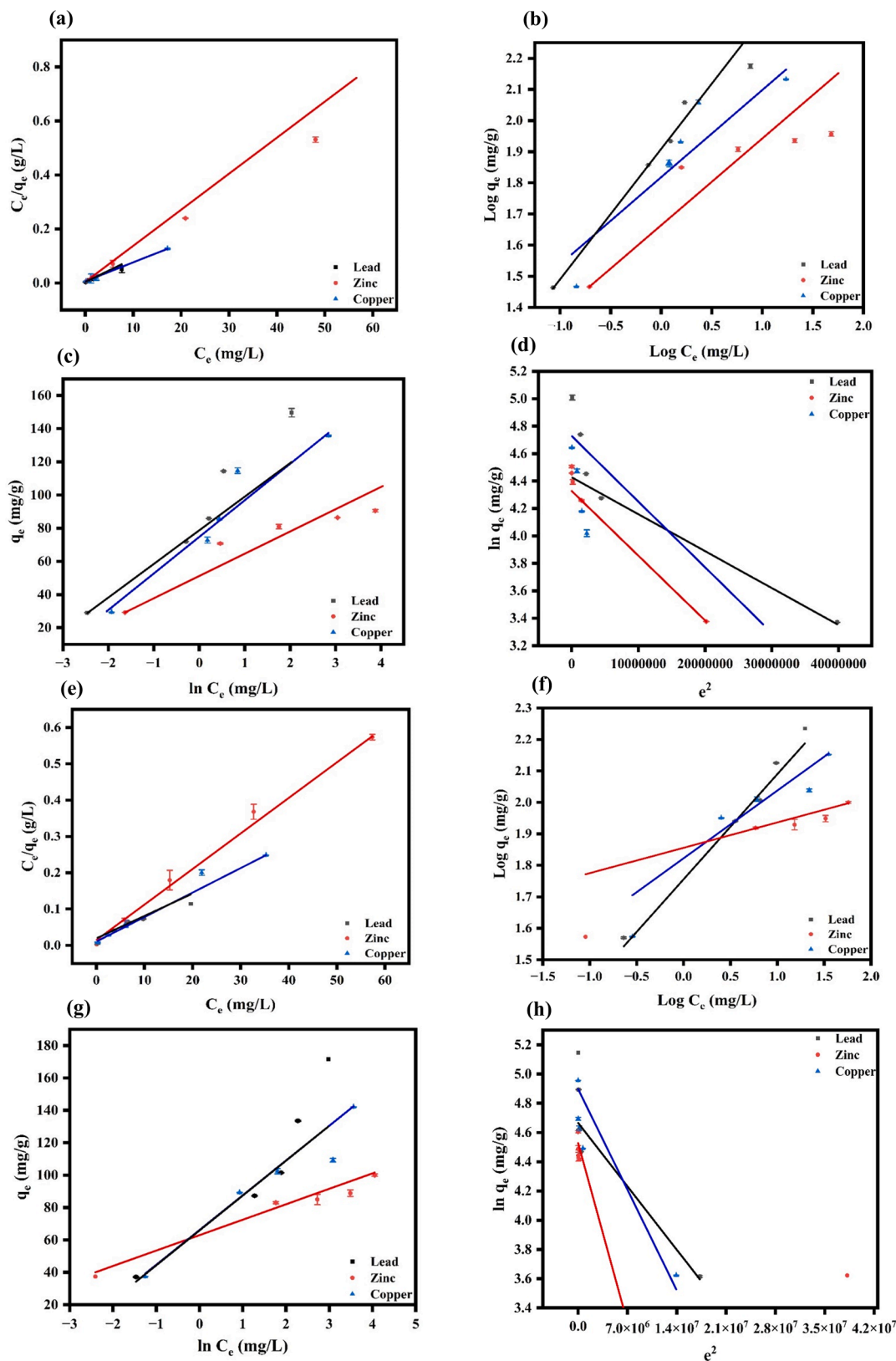


Fig. 7. (a) Langmuir isotherm model fitting using for lead, zinc, and copper using CNF-SP monolithic aerogels, (b) Freundlich isotherm model fitting for lead, zinc, and copper using CNF-SP monolithic aerogels, (c) Temkin isotherm model fitting for lead, zinc, and copper using CNF-SP monolithic aerogels (d) Dubinin-Radushkevich isotherm model fitting for lead, zinc, and copper using CNF-SP monolithic aerogels at (Lead: Co = 20 mg/L, pH = 5, Dose = 0.13 g, T = 25 °C; Zinc: Co = 20 mg/L, pH = 5.5, Dose = 0.13 g, T = 25 °C; Copper: Co = 20 mg/L, pH = 5.5, Dose = 0.13 g, T = 25 °C), (e) Langmuir isotherm model fitting using for lead, zinc, and copper using CNF-SP aerogel beads, (f) Freundlich isotherm model fitting for lead, zinc, and copper using CNF-SP aerogel beads, (g) Temkin isotherm model fitting for lead, zinc, and copper using CNF-SP aerogel beads (h) Dubinin-Radushkevich isotherm model fitting for lead, zinc, and copper using CNF-SP aerogel

beads at (Lead: Co = 20 mg/L, pH = 5, Dose = 0.1 g, T = 25 °C; Zinc: Co = 20 mg/L, pH = 5.5, Dose = 0.1 g, T = 25 °C; Copper: Co = 20 mg/L, pH = 5.5, Dose = 0.1 g, T = 25 °C).

Table 4

Adsorption isotherm parameters for the adsorption of lead, zinc, and copper on CNF-SP aerogel beads.

Isotherm model	Lead	Zinc	Copper
Langmuir	q_m (mg/g) = 191.6 $R_L = 0.031-0.15$ $R^2 = 0.92$	q_m (mg/g) = 100.0 $R_L = 0.014-0.075$ $R^2 = 0.99$	q_m (mg/g) = 139.86 $R_L = 0.018-0.090$ $R^2 = 0.96$
Freundlich	$K_F = 59.14$ $1/n = 0.34$ $R^2 = 0.98$	$K_F = 56.02$ $1/n = 0.15$ $R^2 = 0.95$	$K_F = 58.43$ $1/n = 0.25$ $R^2 = 0.89$
Temkin	B_T (J/mol) = 27.72 A_T (L/g) = 11.52 $R^2 = 0.85$	B_T (J/mol) = 9.26 A_T (L/g) = 730.65 $R^2 = 0.97$	B_T (J/mol) = 19.24 A_T (L/g) = 29.06 $R^2 = 0.92$
Dubinin–Raduskevich	q_s (mg/g) = 120.8 K_{Dr} (mol ² /kJ ²) = 6.9×10^{-8} $E = 2698$ $R^2 = 0.75$	q_s (mg/g) = 89.1 K_{Dr} (mol ² /kJ ²) = 2.3×10^{-8} $E = 4692.1$ $R^2 = 0.96$	q_s (mg/g) = 111.2 K_{Dr} (mol ² /kJ ²) = 7.9×10^{-8} $E = 2519$ $R^2 = 0.88$

isotherm model. This implies that the adsorption of lead occurred on a heterogenous surface with multiple layer formation, and that the distribution of adsorption energies was non-uniform. Alternatively, the experimental data for zinc and copper was in agreement with the Langmuir isotherm model.

7. Adsorption studies in a multi-metal and mixed matrix system

7.1. Effect of background electrolytes

In real wastewater, various other ions exist in addition to heavy metal ions. Therefore, it is important to study the effects of other ions on the adsorption of heavy metals. The existence of other competing ions can affect the adsorption capacity by occupying the active sites due to preferential adsorption. Additionally, the ions can interact and form bonds with the heavy metal ions which have the ability to change the chemistry of the heavy metal ions and prevent their natural adsorption mechanism and interactions with the aerogels [37]. In this study, NaCl and MgCl₂ were used as the model ions to investigate the effect of monovalent and divalent ions on the adsorption of lead, zinc, and copper. According to the results presented in Fig. 8, as the concentration of NaCl and MgCl₂ increased from 0.001 to 0.1 M, an obvious reduction in the percentage removal for all the heavy metals for the monolithic aerogels and the aerogel beads was observed. This could be because of the hindrance in the electrostatic interaction that occurred between the adsorbent and the heavy metal ions by the electrostatic screening effect [38]. Moreover, the Na⁺ and Mg²⁺ ions may be in competition with the heavy metal ions for the active sites. Evidently, MgCl₂ appeared to have a greater influence on the reduction of the removal percentage of all the metals as the concentration increased when compared to NaCl. This may be because of stronger electrostatic interactions caused by the divalent ions when compared to monovalent ions and thereby dominating the active sites more efficiently [37].

7.2. Adsorption studies in a mixed-matrix system, performance comparison with commercially activated carbon and other materials in literature

To further understand the adsorption behaviour in the presence of other contaminants, a mixed matrix system was created with various

concentrations of nitrates, orthophosphate, calcium, ammonia, magnesium, lead, zinc, and copper as shown in Table 5. The removal percentage was studied at a pH of 5 and 5.5 for the monolithic aerogels. According to the adsorption results, the removal percentage of lead, zinc, and copper at a pH of 5 was 98.4 %, 88.4 %, and 93.6 %, respectively. A reduction of 1.2 %, 10.6 %, and 5.7 %, respectively, was observed when compared to the single metal studies. When the pH was increased to 5.5, the removal percentage reduced to 68.3 %, 67.2 %, and 57.1 for lead, zinc, and copper, respectively, indicating that the pH plays a notable role in dictating the adsorption capabilities of the aerogels. Nevertheless, the adsorbent still shows a high removal percentage even in the presence of various other contaminants. Interestingly, the observed selectivity of the heavy metals was as follows: lead (30.3 mg/g) > copper (28.8 mg/g) > zinc (27.2 mg/g). The same selectivity trend was observed when the adsorption studies were conducted with the CNF-SP aerogel beads under optimal conditions in a multi-metal matrix with the removal percentages being 97.9 %, 82.5 %, and 96.7 % and the adsorption capacities being 30.1 mg/g, 25.4 mg/g, and 29.7 mg/g for lead, zinc, and copper, respectively. The selectivity of the heavy metal ions depends on various factors such as the chemical composition, surface charge of the adsorbent and functional groups available for binding the heavy metal ions. In this case, the selectivity can be described in terms of the electronegativity of the heavy metal ions. Generally, lead has a higher electronegativity of 2.33 when compared to copper and zinc that have an electronegativity of 1.90 and 1.65 respectively. As presented in the aforementioned results of the zeta potential, the surface charge during the adsorption process was negative and promoted electrostatic interactions with the heavy metal ions. A higher electronegativity implies a higher affinity for electrons and infers higher specific adsorption [39–41]. Therefore, lead and copper display higher selectivity when compared to zinc. Additionally, the selectivity can also be explained in terms of the hydrated radius. The hydrated radius of lead, zinc and copper is 4.01 Å, 4.30 Å, and 4.19 Å. The smaller hydrated radius of lead and copper allows for the formation of stronger bonds with the available functional groups in comparison to zinc [42].

To further compare the removal percentage of the CNF-SP monolithic aerogels and aerogel beads, commercially available activated carbon was used to test the removal percentage of lead, zinc, and copper from water without any additional contaminants. The removal percentage was calculated to be 16.0 %, 13.2 %, and 26.6 % respectively, and was much lower than the removal percentage achieved by the CNF-SP aerogels even when various other contaminants were present. The aerogels also showed comparatively superior performance when compared to other materials and technologies in literature. For instance, when cellulose/graphene aerogels were used for the removal of heavy metals including lead, zinc, and copper the maximum adsorption capacity was 57.2 mg/g, 69.5 mg/g, and 80.1 mg/g, respectively [43]. Similarly, cellulose/tannic acid based aerogels were used to remove copper from water with an adsorption capacity of 45.6 mg/g [44]. Amino-functionalized cellulose nanocrystal were reported to adsorb lead and copper from water with an adsorption capacity of 54.1 and 49.6 mg/g, respectively [45]. Chitosan/cellulose (CS/CL) nanofibers prepared via electrospinning used to remove lead and copper demonstrated an adsorption capacity of 57.3 mg/g and 112.6 mg/g, respectively [46]. When a membrane-based technology using cellulose nanofibers was used to remove lead and copper from water, the adsorption capacity was 22.0 mg/g and 49.0 mg/g, respectively [47]. When an ozonation technique was used with calcium peroxide the maximum removal percentage was 89.8 %, 93.4 %, and 92.1 % for lead, zinc, and copper, respectively, which was lower in comparison to the results in this study [48].

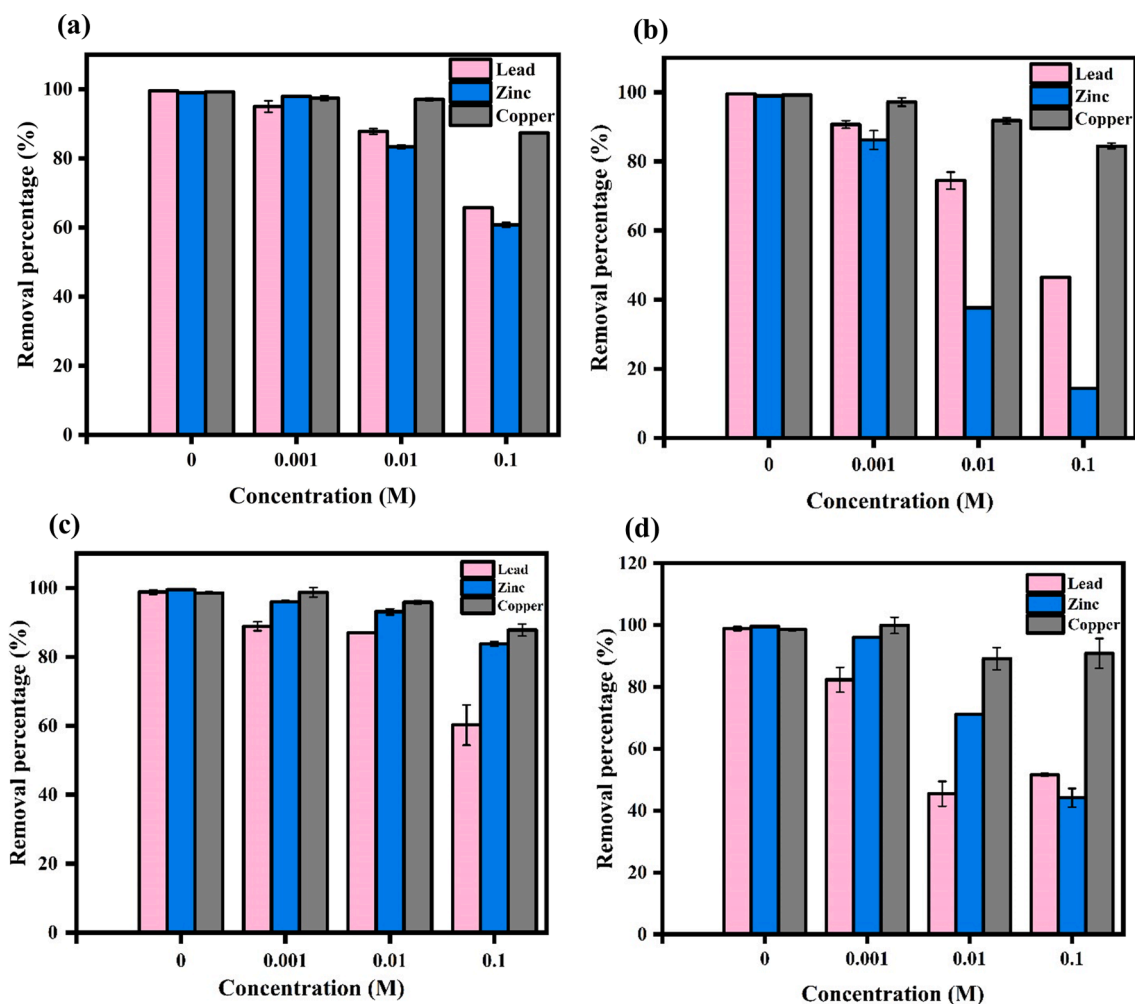


Fig. 8. (a) Effect of NaCl on the removal percentage of lead, zinc and copper using CNF-SP monolithic aerogels, (b) Effect of MgCl₂ on the adsorption of lead, zinc, and copper on CNF-SP monolithic aerogels at (Lead: Co = 20 mg/L, pH = 5, Dose = 0.13 g, T = 25 °C; Zinc: Co = 20 mg/L, pH = 5.5, Dose = 0.13 g, T = 25 °C; Copper: Co = 20 mg/L, pH = 5.5, Dose = 0.13 g, T = 25 °C), (c) Effect of NaCl on the removal percentage of lead, zinc, and copper using CNF-SP aerogel beads, (d) Effect of MgCl₂ on the adsorption of lead, zinc, and copper on CNF-SP aerogel beads at (Lead: Co = 20 mg/L, pH = 5, Dose = 0.1 g, T = 25 °C; Zinc: Co = 20 mg/L, pH = 5.5, Dose = 0.1 g, T = 25 °C; Copper: Co = 20 mg/L, pH = 5.5, Dose = 0.1 g, T = 25 °C).

Table 5

Composition of simulated multi-metal matrix solution.

Heavy metal solution composition	Concentration (mg/L)
NaNO ₃	2.45
Orthophosphate	5.41
Calcium	28.62
Magnesium	7.67
Ammonia	62
Lead	20
Zinc	20
Copper	20

8. Adsorption mechanisms and computational insights

To understand the adsorption mechanisms between heavy metal ions and the CNF-SP aerogels, FTIR analysis was performed after the adsorption process had reached equilibrium to investigate the functional groups participating in the adsorption process as shown in Fig. 9 (h). Interestingly, the peaks at 3341 cm⁻¹, 2900 cm⁻¹, 1594 cm⁻¹, 1476 cm⁻¹, and 1402 cm⁻¹ which were attributed to the O–H stretching vibration from CNF, the C–H stretching vibration in the CNF structure, C=O stretching vibration of amide II from PGA and COO⁻ group band

from SA, N–H bending and the C–N stretching vibrations of the –CO–NH– group from PGA were altered after adsorption in the spectrum of lead, copper, and zinc loaded CNF-SP aerogels. It was observed that the peaks for lead were reduced more significantly than those for zinc and copper. These results are consistent with the higher adsorption capacity of lead in comparison to zinc and copper. Through these observations, it can be concluded that the governing functional groups participating in the adsorption of the heavy metals were the hydroxyl, amino, and carboxyl groups, specifically the oxygen and nitrogen containing groups. When the functional groups interact with the heavy metal ions, they can form coordination bonds with the heavy metals, form metal complexes and facilitate electron transfer. Moreover, the zeta potential of a material gives valuable insights into the possible adsorption mechanism between the adsorbent and adsorbate. As previously mentioned, the measured zeta potential at the optimal pH was negative. Therefore, electrostatic interactions between the negative surface and the positively charged cations can be initiated.

To further understand the reactions between the heavy metal ions and the CNF-SP aerogels, DFT calculations were performed. Investigating the interaction of heavy metal ions with the functional groups present on the aerogels is valuable for interpreting competitive adsorption. As shown in Fig. 9 (b), (c), and (d), the optimized geometries suggest that oxygen and nitrogen containing groups were mainly

involved in the adsorption process. Previously, it has been reported and established that the value of the adsorption energy can be used to uncover if the adsorption mechanism was governed by physical adsorption or chemisorption [49]. Typically, if the value of the adsorption energy is

greater than 0 eV, the adsorption is considered unfavourable and denotes that adsorption cannot take place upon interaction with the adsorbent. If the value of the adsorption energy is between 0 and -0.2 eV, it is concluded that the means of adsorption is physical adsorption.

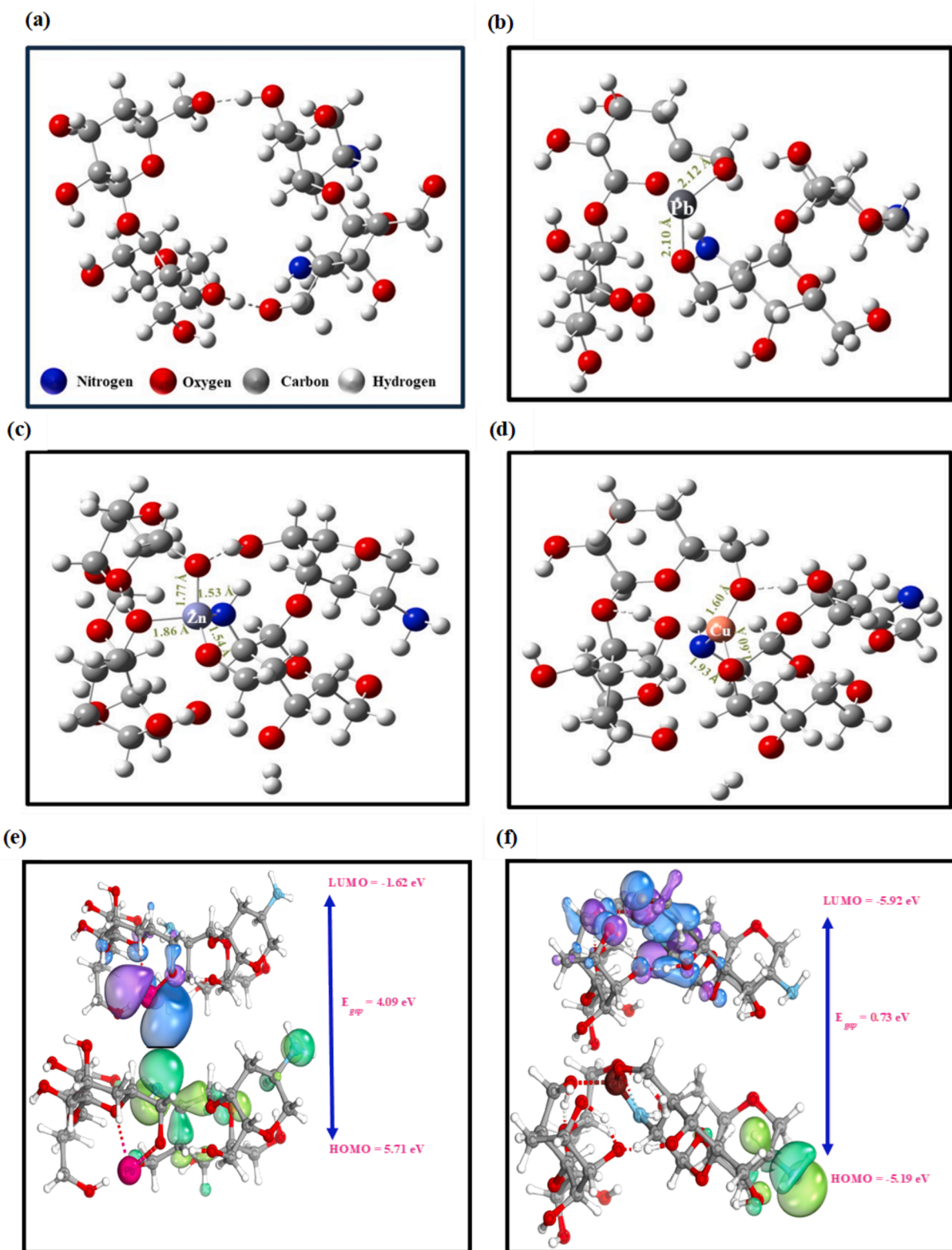


Fig. 9. (a) Optimized structure of CNF-SP aerogels, (b) Optimized structure of CNF-SP-Pb, (c) Optimized structure of CNF-SP-Zn, (d) Optimized structure of CNF-SP-Cu, (e) HOMO-LUMO plots of CNF-SP-Pb, (f) HOMO-LUMO plots of CNF-SP-Zn, (g) HOMO-LUMO plots of CNF-SP-Cu, (h) FTIR spectrum of CNF-SP monolithic aerogels after adsorption of lead, zinc, and copper.

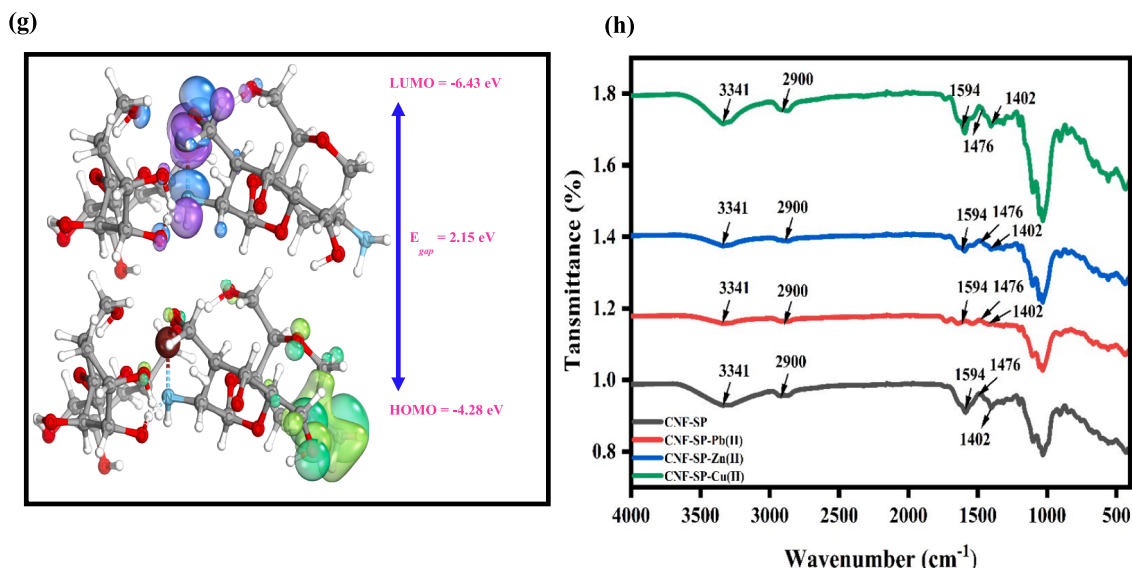


Fig. 9. (continued).

Table 6

Quantum chemical parameters of CNF-SP aerogels, CNF-SP-Pb, CNF-SP-Zn and CNF-SP-Cu.

Molecule	HOMO (eV)	LUMO (eV)	E_{gap} (eV)	HOMO (eV)	LUMO (eV)	Chemical hardness (η)	Chemical softness (S)
CNF	6.65	1.19	5.45	6.65	1.19	2.73	0.37
CNF-Pb	-1.62	-5.71	4.09	1.62	5.71	2.05	0.49
CNF-Zn	-5.19	-5.92	0.73	5.19	5.92	0.36	2.76
CNF-Cu	-4.28	-6.43	2.15	4.28	6.43	1.079	0.93

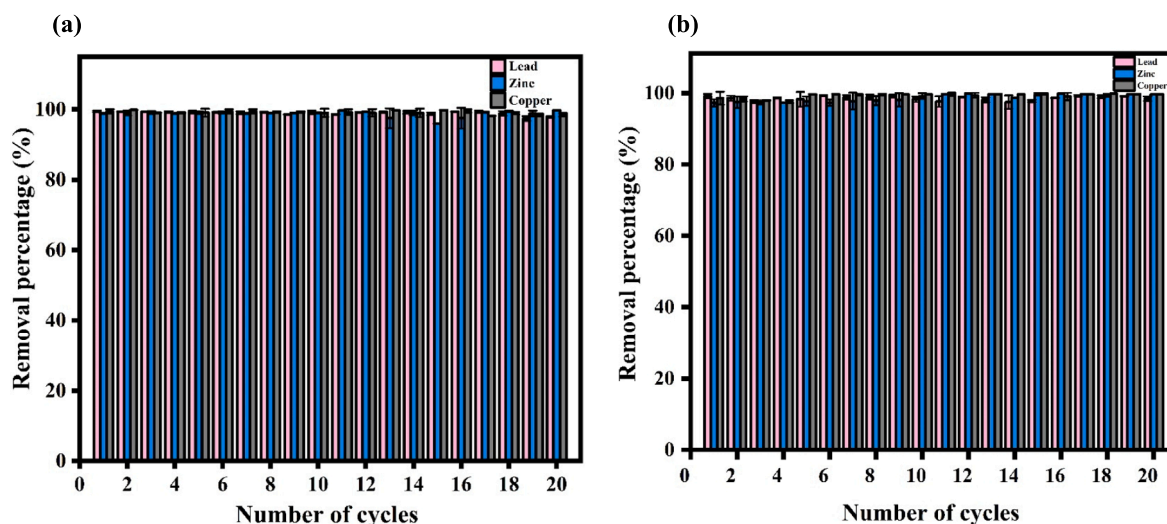


Fig. 10. (a) Adsorption-desorption cycles for CNF-SP monolithic aerogels (Lead: Co = 20 mg/L, pH = 5, Dose = 0.13 g, T = 25 °C; Zinc: Co = 20 mg/L, pH = 5.5, Dose = 0.13 g, T = 25 °C; Copper: Co = 20 mg/L, pH = 5.5, Dose = 0.13 g, T = 25 °C) (b) Adsorption-desorption cycles for CNF-SP aerogel beads (Lead: Co = 20 mg/L, pH = 5, Dose = 0.1 g, T = 25 °C; Zinc: Co = 20 mg/L, pH = 5.5, Dose = 0.1 g, T = 25 °C; Copper: Co = 20 mg/L, pH = 5.5, Dose = 0.1 g, T = 25 °C).

Alternatively, when the value of the adsorption energy is less than -0.5 eV, the adsorption takes place through chemisorption [5]. As shown in Fig. 9 (a), (b), (c), and (d), the adsorption energies were explored to understand the adsorption mechanism. The adsorption energies in this study for lead, zinc, and copper were -345.0 eV, -335.1 eV and -340 eV, respectively. It is apparent that chemisorption was the governing adsorption mechanism in the study for all the heavy metals. This conclusion is also in accordance with the results attained from the adsorption kinetics study. Moreover, the adsorption energies also give

an insight into the preferential adsorption on the aerogels. A more negative adsorption energy signifies a stronger interaction between the heavy metal ion and the adsorbent. The order of adsorption energies in view of the most negative value was lead > copper > zinc. In this study, the adsorption energy of lead was more negative compared to copper and zinc. The trend is in alignment with the experimental results acquired through the adsorption studies.

The ability to gain or donate electrons can be described in terms of the highest occupied molecular orbital (HOMO) and the least

unoccupied molecular orbital (LUMO). A high HOMO value indicates that the molecule is prone to losing electrons more easily, whereas a lower LUMO value indicates that the molecule can easily receive electrons. According to the values in Table 6 and Fig. 9. (e), (f), and (g), the higher HOMO value for the CNF-SP aerogels suggests that they may act as electron donors and facilitate electron transfer and potentially form coordinate bonds between the heavy metal ions and the oxygen and nitrogen containing groups through the overlapping of their orbitals. Additionally, the difference between LUMO and HOMO, also known as energy gap (E_{gap}) can provide insights into the ease with which a molecule can be excited. E_{gap} can describe the capability of an electron to transition from an occupied orbital to an unoccupied orbital. According to Fig. 9 (e), (f), and (g) and Table 6, the energy gaps of the metal-aerogel complex after the adsorption of the heavy metal ions are lower than that of the CNF-SP aerogel. The data implies that the aerogel was stabilised after interacting with the heavy metal ions. Additionally, a complex with a larger E_{gap} represents more stability when compared to a complex with a smaller E_{gap} because molecular systems with a narrow band exhibit reduced resistance to electron cloud polarization when interacting with adsorbates [50]. In this study, the lead complex exhibited the largest E_{gap} value, suggesting that it was the most stable complex. The larger E_{gap} of lead suggests that the chemical interaction between lead and the aerogel was stronger in comparison to copper and zinc. This analysis can further strengthen the evidence for the higher adsorption capacity and preferential adsorption of lead over copper and zinc in both single-metal and multi-metal scenarios. To further analyse the properties of the complexes, the chemical hardness was calculated. Chemical hardness is also associated with the stability of a structure. The higher the value of the chemical hardness, the more stable and resistant the structure is to changes in electron density [49]. It is clear from Table 6 that the chemical hardness of the CNF-SP complex is higher than the chemical softness, indicating the stability of the adsorbent. Moreover, the CNF-SP-lead complex has the highest chemical hardness and therefore is more stable when compared to the CNF-SP-zinc complex and CNF-SP copper complex.

9. Desorption and regeneration potential of CNF-SP monolithic aerogels and CNF-SP aerogel beads

To reduce the overall cost of the adsorption process and to minimize the environmental impact of the adsorbents, it is essential to study the regeneration potential of the adsorbents. In this study, 1 M citric acid solution was chosen as the eluent to desorb the adsorbed heavy metal ions from the CNF-SP monolithic aerogels and the aerogel beads as presented in Fig. 10. With 1 M citric acid, the desorption efficiency even in the 19th cycle could be maintained above 97 % for both monoliths and aerogel beads. Compared to other common eluents such as nitric acid, hydrochloric acid, and sodium hydroxide, citric acid is considered as a weak organic acid. In general, it is less toxic to the environment in comparison to the aforementioned eluents. Moreover, due to its weaker nature, it is expected that the possibility of any substantial structural damage to the aerogels will be reduced. The recyclability of the CNF-SP monolithic aerogels and aerogel beads using citric acid as an eluent was remarkable. The CNF-SP monolithic aerogels and aerogel beads could be recycled 20 times without any notable change in the removal percentage of the heavy metal ions even in the 20th cycle. Overall, the percentage removal of all the heavy metals in the adsorption–desorption cycles could be maintained above 97 % throughout the 20 cycles. Moreover, the aerogels could maintain their shape as shown in Fig. S2 (a) and (b). The excellent ability of the aerogels to retain their adsorption capability and shape demonstrates their promising potential to be employed for practical applications.

10. Conclusion

This study focuses on preparing sustainable and highly regenerative

aerogels using non-toxic biopolymers such as sodium alginate, polyglutamic acid and cellulose nanofibers. The aerogels were prepared in the form of monoliths and beads through a simple freeze-drying process. The aerogel beads showed superior physical characteristics in terms of their specific surface area. The specific surface areas of the monolithic aerogels and aerogel beads were found to be 227 m²/g and 258 m²/g, respectively. Furthermore, the SEM analysis depicted that the aerogel beads had a highly interconnected network in comparison to the monolithic aerogels. The aerogel beads displayed superior adsorption capacity with maximum values of 171.7 mg/g, 100.0 mg/g, and 142.0 mg/g for lead, zinc, and copper, respectively. Both types of aerogels followed pseudo-second-order kinetics and also the Elovich model in the case of lead when monolithic aerogels were used, implying that the governing mechanism was chemical adsorption. These results were further confirmed through DFT calculations. Multi-matrix studies disclosed that the aerogels performed well even in the presence of various other contaminants and could remove more than 93 % of lead and copper and more than 82 % of zinc in both monolithic aerogel and aerogel bead configuration. The aerogels showed remarkable regenerative abilities and were recycled 20 times with no significant reduction in the adsorption performance.

CRediT authorship contribution statement

Hina Iqbal Syeda: Writing – review & editing, Writing – original draft, Methodology, Investigation, Conceptualization. **Shobha Muthukumaran:** Writing – review & editing, Writing – original draft. **Kanagaratnam Baskaran:** Writing – review & editing, Writing – original draft.

Declaration of competing interest

The authors declare that they have no known competing financial interests or personal relationships that could have appeared to influence the work reported in this paper.

Data availability

Data will be made available on request.

Acknowledgements

Hina Iqbal Syeda acknowledges Deakin university for the Deakin University Postgraduate Research Scholarship (DUPR).

Appendix A. Supplementary data

Supplementary data to this article can be found online at <https://doi.org/10.1016/j.seppur.2024.128311>.

References

- [1] A.G. Adeniyi, J.O. Ighalo, Biosorption of pollutants by plant leaves: an empirical review, *J. Environ. Chem. Eng.* 7 (2019) 103100, <https://doi.org/10.1016/j.jece.2019.103100>.
- [2] M. Jaishankar, T. Tseten, N. Anbalagan, B.B. Mathew, K.N. Beeregowda, Toxicity, mechanism and health effects of some heavy metals, *Interdiscip. Toxicol.* 7 (2014) 60–72, <https://doi.org/10.2478/intox-2014-0009>.
- [3] O.B. Akpor, Heavy metal pollutants in wastewater effluents: sources, effects and remediation, *Adv. Biosci. Bioeng.* 2 (2014) 37, <https://doi.org/10.11648/j.abb.20140204.11>.
- [4] Z. Zheng, J. Liu, M. Zhang, H. Li, J. Pan, A crescent-shaped imprinted microgel adsorbent with near-infrared light-responsive performance for selective adsorption of Lead(II), *Sep. Purif. Technol.* 328 (2024) 124963, <https://doi.org/10.1016/j.seppur.2023.124963>.
- [5] B. Wang, Z. Bai, H. Jiang, P. Prinsen, R. Luque, S. Zhao, J. Xuan, Selective heavy metal removal and water purification by microfluidically-generated chitosan microspheres: characteristics, modeling and application, *J. Hazard. Mater.* 364 (2019) 192–205, <https://doi.org/10.1016/j.jhazmat.2018.10.024>.

- [6] W. Maatar, S. Boufi, Poly(methacrylic acid-co-maleic acid) grafted nanofibrillated cellulose as a reusable novel heavy metal ions adsorbent, *Carbohydr. Polym.* 126 (2015) 199–207, <https://doi.org/10.1016/j.carbpol.2015.03.015>.
- [7] L.N. Tan, N.C.T. Nguyen, A.M.H. Trinh, N.H.N. Do, K.A. Le, P.K. Le, Eco-friendly synthesis of durable aerogel composites from chitosan and pineapple leaf-based cellulose for Cr(VI) removal, *Sep. Purif. Technol.* 304 (2023), <https://doi.org/10.1016/j.seppur.2022.122415>.
- [8] M.K. Goswami, A. Srivastava, R.K. Dohare, A.K. Tiwari, A. Srivastav, Recent advances in conducting polymer-based magnetic nanosorbents for dyes and heavy metal removal: fabrication, applications, and perspective, *Environ. Sci. Pollut. Res.* 30 (2023) 73031–73060, <https://doi.org/10.1007/s11356-023-27458-4>.
- [9] M. Yuan, D. Liu, S. Shang, Z. Song, Q. You, L. Huang, S. Cui, A novel magnetic Fe₃O₄/cellulose nanofiber/polyethyleneimine/thiol-modified montmorillonite aerogel for efficient removal of heavy metal ions: adsorption behavior and mechanism study, *Int. J. Biol. Macromol.* 253 (2023) 126634, <https://doi.org/10.1016/j.ijbiomac.2023.126634>.
- [10] M. Maharana, S. Sen, Magnetic zeolite: a green reusable adsorbent in wastewater treatment, *Mater. Today Proc.* 47 (2021) 1490–1495, <https://doi.org/10.1016/j.matpr.2021.04.370>.
- [11] A. Chatla, I.W. Almanassra, L. Jaber, V. Kochkodan, T. Laoui, H. Alawadhi, M. A. Atieh, Influence of calcination atmosphere on Fe doped activated carbon for the application of lead removal from water, *Colloids Surf. A Physicochem. Eng. Asp.* 652 (2022) 129928, <https://doi.org/10.1016/j.colsurfa.2022.129928>.
- [12] I.W. Almanassra, T. Al-Ansari, I. Ihsanullah, V. Kochkodan, A. Chatla, M.A. Atieh, A. Shanableh, T. Laoui, Carbide-derived carbon as an extraordinary material for the removal of chromium from an aqueous solution, *Chemosphere* 307 (2022) 135953, <https://doi.org/10.1016/j.chemosphere.2022.135953>.
- [13] V. thi Quyen, T.H. Pham, J. Kim, D.M. Thanh, P.Q. Thang, Q. Van Le, S.H. Jung, T. Y. Kim, Biosorbent derived from coffee husk for efficient removal of toxic heavy metals from wastewater, *Chemosphere* 284 (2021) 131312, <https://doi.org/10.1016/j.chemosphere.2021.131312>.
- [14] F. Batool, A. Mohyuddin, A. Amjad, A. ul Hassan, S. Nadeem, M. Javed, M. Hafiz Dzarfan Othman, K. Wayne Chew, A. Rauf, T.A. Kurniawan, Removal of Cd(II) and Pb(II) from synthetic wastewater using Rosa damascena waste as a biosorbent: an insight into adsorption mechanisms, kinetics, and thermodynamic studies, *Chem. Eng. Sci.* 280 (2023), <https://doi.org/10.1016/j.ces.2023.119072>.
- [15] I.W. Almanassra, A. Chatla, Y. Zakaria, V. Kochkodan, A. Shanableh, T. Laoui, M. A. Atieh, Palm leaves based biochar: advanced material characterization and heavy metal adsorption study, *Biomass Convers. Biorefinery.* (2022), <https://doi.org/10.1007/s13399-022-03590-y>.
- [16] J. Li, S. Tan, Z. Xu, Anisotropic nanocellulose aerogel loaded with modified uio-66 as efficient adsorbent for heavy metal ions removal, *Nanomaterials.* 10 (2020) 1–13, <https://doi.org/10.3390/nano10061114>.
- [17] K. Dhali, M. Ghasemlou, F. Daver, P. Cass, B. Adhikari, A review of nanocellulose as a new material towards environmental sustainability, *Sci. Total Environ.* 775 (2021) 145871, <https://doi.org/10.1016/j.scitotenv.2021.145871>.
- [18] H. Iqbal, S. Muthukumar, K. Baskaran, Shape-memory cellulose nanofiber / polyglutamic acid-based aerogels as novel adsorbents for the removal of heavy metals from aqueous solutions, *J. Water Process Eng.* 58 (2024) 104780, <https://doi.org/10.1016/j.jwpe.2024.104780>.
- [19] N. Rong, C. Chen, K. Ouyang, K. Zhang, X. Wang, Z. Xu, Adsorption characteristics of directional cellulose nanofiber/chitosan/montmorillonite aerogel as adsorbent for wastewater treatment, *Sep. Purif. Technol.* 274 (2021) 119120, <https://doi.org/10.1016/j.seppur.2021.119120>.
- [20] C. Tang, P. Brodie, Y. Li, N.J. Grishkewich, M. Brunsting, K.C. Tam, Shape recoverable and mechanically robust cellulose aerogel beads for efficient removal of copper ions, *Chem. Eng. J.* 392 (2020) 124821, <https://doi.org/10.1016/j.cej.2020.124821>.
- [21] C. Tang, P. Brodie, M. Brunsting, K.C. Tam, Carboxylated cellulose cryogel beads via a one-step ester crosslinking of maleic anhydride for copper ions removal, *Carbohydr. Polym.* 242 (2020) 116397, <https://doi.org/10.1016/j.carbpol.2020.116397>.
- [22] M. Sorriaux, M. Sorieul, Y. Chen, Bio-based and robust polydopamine coated nanocellulose/ amyloid composite aerogel for fast and wide-spectrum water purification, *Polymers (Basel)* 13 (2021), <https://doi.org/10.3390/polym13193442>.
- [23] Q. Liu, Y. Liu, Q. Feng, C.C. Chen, Z. Xu, Preparation of antifouling and highly hydrophobic cellulose nanofibers/alginate aerogels by bidirectional freeze-drying for water-oil separation in the ocean environment, *J. Hazard. Mater.* 441 (2023) 129965, <https://doi.org/10.1016/j.jhazmat.2022.129965>.
- [24] S. Alila, A.M. Ferrara, A.M. Botelho do Rego, S. Boufi, Controlled surface modification of cellulose fibers by amino derivatives using N, N'-carbonyldiimidazole as activator, *Carbohydr. Polym.* 77 (2009) 553–562, <https://doi.org/10.1016/j.carbpol.2009.01.028>.
- [25] M. Li, C. Tang, S. Fu, K.C. Tam, Y. Zong, Cellulose-based aerogel beads for efficient adsorption- reduction- sequestration of Cr(VI), *Int. J. Biol. Macromol.* 216 (2022) 860–870, <https://doi.org/10.1016/j.ijbiomac.2022.07.215>.
- [26] J.C. Antunes, C.L. Pereira, M. Molinos, F. Ferreira-Da-Silva, M. Dessi, A. Gloria, L. Ambrosio, R.M. Gonçalves, M.A. Barbosa, Layer-by-layer self-assembly of chitosan and poly(γ -glutamic acid) into polyelectrolyte complexes, *Biomacromolecules.* 12 (2011) 4183–4195, <https://doi.org/10.1021/bm2008235>.
- [27] L. Mo, H. Pang, Y. Lu, Z. Li, H. Kang, M. Wang, S. Zhang, J. Li, Wood-inspired nanocellulose aerogel adsorbents with excellent selective pollutants capture, superfast adsorption, and easy regeneration, *J. Hazard. Mater.* 415 (2021) 125612, <https://doi.org/10.1016/j.jhazmat.2021.125612>.
- [28] K. Huang, H. Zhu, Removal of Pb²⁺ from aqueous solution by adsorption on chemically modified muskmelon peel, *Environ. Sci. Pollut. Res.* 20 (2013) 4424–4434, <https://doi.org/10.1007/s11356-012-1361-7>.
- [29] L. Mo, H. Pang, Y. Tan, S. Zhang, J. Li, 3D Multi-wall Perforated Nanocellulose-Based Polyethyleneimine Aerogels for Ultrahigh Efficient and Reversible Removal of Cu(II) Ions from Water, *Chem. Eng. J.* 378 (2019) 122157, <https://doi.org/10.1016/j.cej.2019.122157>.
- [30] S.E.A. Elhafez, H.A. Hamad, A.A. Zaatout, G.F. Malash, Management of agricultural waste for removal of heavy metals from aqueous solution: adsorption behaviors, adsorption mechanisms, environmental protection, and techno-economic analysis, *Environ. Sci. Pollut. Res.* 24 (2017) 1397–1415, <https://doi.org/10.1007/s11356-016-7891-7>.
- [31] H. Guo, S. Zhang, Z. Kou, S. Zhai, W. Ma, Y. Yang, Removal of cadmium(II) from aqueous solutions by chemically modified maize straw, *Carbohydr. Polym.* 115 (2015) 177–185, <https://doi.org/10.1016/j.carbpol.2014.08.041>.
- [32] A.A. Edathil, I. Shittu, J.H. Zain, F. Banat, M.A. Haija, Novel magnetic coffee waste nanocomposite as effective bioadsorbent for Pb(II) removal from aqueous solutions, *J. Environ. Chem. Eng.* 6 (2018) 2390–2400, <https://doi.org/10.1016/j.jece.2018.03.041>.
- [33] K.W. Jung, S.Y. Lee, Y.J. Lee, Hydrothermal synthesis of hierarchically structured birnessite-type MnO₂/biochar composites for the adsorptive removal of Cu(II) from aqueous media, *Bioresour. Technol.* 260 (2018) 204–212, <https://doi.org/10.1016/j.biortech.2018.03.125>.
- [34] B. Kalebčić, A. Bafit, H. Cajner, M. Marcius, G. Matijašić, L. Čurković, Optimization of Ciprofloxacin Adsorption on Clinoptilolite-Based Adsorbents Using Response Surface Methodology, *Nanomaterials.* 13 (2023), <https://doi.org/10.3390/nano13040740>.
- [35] T.H. Pham, S.H. Jung, Y.J. Kim, T.Y. Kim, Adsorptive removal and recovery of organic pollutants from wastewater using waste paper-derived carbon-based aerogel, *Chemosphere.* 268 (2021) 129319, <https://doi.org/10.1016/j.chemosphere.2020.129319>.
- [36] J. Ma, J. Li, Q. Guo, H. Han, S. Zhang, R. Han, Waste peanut shell modified with polyethyleneimine for enhancement of hexavalent chromium removal from solution in batch and column modes, *Bioresour. Technol. Reports.* 12 (2020) 100576, <https://doi.org/10.1016/j.biteb.2020.100576>.
- [37] X. Lin, T. Shen, M. Li, J. Shaoyu, W. Zhuang, M. Li, H. Xu, C. Zhu, H. Ying, P. Ouyang, Synthesis, characterization, and utilization of poly-amino acid-functionalized lignin for efficient and selective removal of lead ion from aqueous solution, *J. Clean. Prod.* 347 (2022) 131219, <https://doi.org/10.1016/j.jclepro.2022.131219>.
- [38] R.Z. Wang, D.L. Huang, Y.G. Liu, C. Zhang, C. Lai, X. Wang, G.M. Zeng, Q. Zhang, X.M. Gong, P. Xu, Synergistic removal of copper and tetracycline from aqueous solution by steam-activated bamboo-derived biochar, *J. Hazard. Mater.* 384 (2020) 121470, <https://doi.org/10.1016/j.jhazmat.2019.121470>.
- [39] Y. Deng, S. Huang, D.A. Laird, X. Wang, Z. Meng, Adsorption behaviour and mechanisms of cadmium and nickel on rice straw biochars in single- and binary-metal systems, *Chemosphere.* 218 (2019) 308–318, <https://doi.org/10.1016/j.chemosphere.2018.11.081>.
- [40] M. Kajeiou, A. Alem, S. Mezghich, N.D. Ahfir, M. Mignot, C. Devouge-Boyer, A. Pantet, Competitive and non-competitive zinc, copper and lead biosorption from aqueous solutions onto flax fibers, *Chemosphere.* 260 (2020), <https://doi.org/10.1016/j.chemosphere.2020.127505>.
- [41] T. Shi, S. Jia, Y. Chen, Y. Wen, C. Du, H. Guo, Z. Wang, Adsorption of Pb(II), Cr(III), Cu(II), Cd(II) and Ni(II) onto a vanadium mine tailing from aqueous solution, *J. Hazard. Mater.* 169 (2009) 838–846, <https://doi.org/10.1016/j.jhazmat.2009.04.020>.
- [42] J.H. Park, Y.S. Ok, S.H. Kim, J.S. Cho, J.S. Heo, R.D. Delaune, D.C. Seo, Competitive adsorption of heavy metals onto sesame straw biochar in aqueous solutions, *Chemosphere.* 142 (2016) 77–83, <https://doi.org/10.1016/j.chemosphere.2015.05.093>.
- [43] P. Sun, M. Wang, T. Wu, L. Guo, W. Han, Covalent Crosslinking Cellulose/ Graphene Aerogels with High Elasticity and Adsorbability for Heavy Metal Ions Adsorption, *Polymers (basel).* 15 (2023), <https://doi.org/10.3390/polym15112434>.
- [44] Y. Ji, Y. Wen, Z. Wang, S. Zhang, M. Guo, Eco-friendly fabrication of a cost-effective cellulose nanofiber-based aerogel for multifunctional applications in Cu (II) and organic pollutants removal, *J. Clean. Prod.* 255 (2020), <https://doi.org/10.1016/j.jclepro.2020.120276>.
- [45] Q. Xu, X. Huang, L. Guo, Y. Wang, L. Jin, Enhancing removal of Cr(VI), Pb²⁺, and Cu²⁺ from aqueous solutions using amino-functionalized cellulose nanocrystal, *Molecules.* 26 (2021), <https://doi.org/10.3390/molecules26237315>.
- [46] D.N. Phan, H. Lee, B. Huang, Y. Mukai, I.S. Kim, Fabrication of electrospun chitosan/cellulose nanofibers having adsorption property with enhanced mechanical property, *Cellulose.* 26 (2019) 1781–1793, <https://doi.org/10.1007/s10570-018-2169-5>.
- [47] H.Y. Choi, J.H. Bae, Y. Hasegawa, S. An, I.S. Kim, H. Lee, M. Kim, Thiol-functionalized cellulose nanofiber membranes for the effective adsorption of heavy

- metal ions in water, *Carbohydr. Polym.* 234 (2020) 115881, <https://doi.org/10.1016/j.carbpol.2020.115881>.
- [48] Z. Honarmandrad, N. Javid, M. Malakootian, Efficiency of ozonation process with calcium peroxide in removing heavy metals (Pb, Cu, Zn, Ni, Cd) from aqueous solutions, *SN Appl. Sci.* 2 (2020) 1–7, <https://doi.org/10.1007/s42452-020-2392-1>.
- [49] S. Kaviani, D.A. Tayurskii, O.V. Nedopekin, I. Piyanzina, DFT insight into Cd²⁺, Hg²⁺, Pb²⁺, Sn²⁺, As³⁺, Sb³⁺, and Cr³⁺ heavy metal ions adsorption onto surface of bowl-like B30 nanosheet, *J. Mol. Liq.* 365 (2022) 120131, <https://doi.org/10.1016/j.molliq.2022.120131>.
- [50] H.R. Ghenaatian, M. Shakourian-Fard, G. Kamath, The effect of sulfur and nitrogen/sulfur co-doping in graphene surface on the adsorption of toxic heavy metals (Cd, Hg, Pb), *J. Mater. Sci.* 54 (2019) 13175–13189, <https://doi.org/10.1007/s10853-019-03791-3>.
- [51] Q. Xie, Y. Zou, Y. Wang, H. Wang, Z. Du, X. Cheng, Mechanically robust sodium alginate/cellulose nanofibers/polyethyleneimine composite aerogel for effective removal of hexavalent chromium and anionic dyes, *Polym. Eng. Sci.* 62 (2022) 1927–1940, <https://doi.org/10.1002/pen.25976>.